04) that had been immunized with the live attenuated vaccine strain SIVmac239Δnef (Fig. 6). In contrast, detection of gp120-binding and gp140-binding B cells was about 10-fold lower in lymphocytes prepared in parallel from naïve uninfected (SIV-negative) macaques, which is likely to represent non-specific binding (Fig. 6). These results demonstrate the utility of biotinylated gp120 and gp140 for specific detection and phenotyping of SIV Env-specific $CD20^{+}IgG^{+}$ B cells. It is noteworthy that the number of gp120 or gp140 $CD20^{+}$ IgG^{+} B detected cells was not particularly increased (less than double) with higher protein concentrations (up to 60 μg/ml). It is possible that Env-specific B cells in the peripheral blood reach an optimum number during the chronic phase for a sterilely protected SIVmac239Δnef immunized macaque with low titer of vaccine strain. A longitudinal study and comparison with other group of SIV infected macaque could provide more clarification on that matter.

4. Conclusion

Sterile protection induced by SIVmac239Δnef in the SIV/macaque model has been extensively studied, but the mechanism of protection remains poorly understood (Mansfield et al., 2008; Gauduin et al., 2006, 1998, 1999a,b). The exact contribution of the commonly studied parameters (such as anti-viral memory T cells, gag specific IFN-γ, binding and neutralizing antibodies) remain unclear. Importantly, characterization of the virus-specific antibody response to SIV infection or vaccination with SIV-based immunogens has been hampered by the lack of reagents for identifying SIV-specific B-lymphocytes. In the current study we demonstrated that soluble SIVmac239 gp140 forms oligomers without the need for additional modifications, and has characteristics similar to those of engineered soluble HIV gp140 (Doria-Rose et al., 2009; Scheid et al., 2009a,b). This soluble SIV gp140 is capable of depleting Env-specific antibodies from the plasma from an animal immunized with SIVmac239Δnef as well as or better than soluble gp120. Importantly, both soluble SIV gp120 and SIV gp140 allowed the identification of SIV-specific B lymphocytes in animals vaccinated with the replication-competent, attenuated vaccine strain SIVmac239Δnef.

These novel tools will be helpful for identification, phenotyping and quantification of ENV-specific B cells (including memory and plasma cells) as previously demonstrated with HIV-1 gp140 (Doria-Rose et al., 2009; Scheid et al., 2009a,b). As with HIV-1 gp140, SIV gp140 should permit the single-cell sorting and cloning of SIV-specific monoclonal antibodies. Importantly, SIV gp120 and SIV gp140 can be used to monitor the dynamics of ENV-specific B cell subsets during the course of SIV infection and in response to vaccination and challenge in SIV/macaque AIDS vaccine studies.

Supplementary materials related to this article can be found online at doi:10.1016/j.jim.2011.05.010.

Acknowledgments

We thank Mackenzie Bartlett for technical assistance. Purified non-conjugated anti-CD4 antibody and anti-CD19 antibody were kind gifts from the NIH Nonhuman Primate Reagent Resource (nhpreagents.bidmc.harvard.edu/NHP/default.aspx). This research was supported by NIH grants AI083118 and AI057039 (WEJ), AI07306 (RPJ) and RR00168 (NEPRC), a grant from the Japan Health Sciences Foundation (H.S.), and a grant from the International AIDS Vaccine Initiative (RPJ). RKR is supported by a CHAVI/HVTN Early Career Investigation award (U19 AI 067854–04).

References

Binley, J.M., et al., 2000. A recombinant human immunodeficiency virus type 1 envelope glycoprotein complex stabilized by an intermolecular disulfide bond between the gp120 and gp41 subunits is an antigenic mimic of the trimeric virion-associated structure. J. Virol. 74 (2), 627.

Browning, J., et al., 1997. Mice transgenic for human CD4 and CCR5 are susceptible to HIV infection. Proc. Natl. Acad. Sci. U. S. A. 94 (26), 14637.

Cole, K.S., et al., 2001. Characterization of neutralization epitopes of simian immunodeficiency virus (SIV) recognized by rhesus monoclonal antibodies derived from monkeys infected with an attenuated SIV strain. Virology 290 (1), 59.

Doria-Rose, N.A., et al., 2009. Frequency and phenotype of human immunodeficiency virus envelope-specific B cells from patients with broadly cross-neutralizing antibodies. J. Virol. 83 (1), 188.

Dykhuizen, M., et al., 1998. Determinants of disease in the simian immunodeficiency virus-infected rhesus macaque: characterizing animals with low antibody responses and rapid progression. J. Gen. Virol. 79 (Pt 10), 2461.

Edinger, A.L., et al., 2000. Characterization and epitope mapping of neutralizing monoclonal antibodies produced by immunization with oligomeric simian immunodeficiency virus envelope protein. J. Virol. 74 (17), 7922.

Farzan, M., et al., 1998. Stabilization of human immunodeficiency virus type 1 envelope glycoprotein trimers by disulfide bonds introduced into the gp41 glycoprotein ectodomain. J. Virol. 72 (9), 7620.

Gauduin, M.C., et al., 1998. Inhibition of simian immunodeficiency virus (SIV) replication by CD8(+) T lymphocytes from macaques immunized with live attenuated SIV. J. Virol. 72 (8), 6315.

Gauduin, M.C., et al., 1999a. Characterization of SIV-specific CD4+ T-helper proliferative responses in macaques immunized with live-attenuated SIV. J. Med. Primatol. 28 (4–5), 233.

Gauduin, M.C., et al., 1999b. Immunization with live attenuated simian immunodeficiency virus induces strong type 1T helper responses and beta-chemokine production. Proc. Natl. Acad. Sci. U. S. A. 96 (24), 14031.

Gauduin, M.C., et al., 2006. Induction of a virus-specific effector-memory CD4+ T cell response by attenuated SIV infection. J. Exp. Med. 203 (12), 2661.

Gray, E.S., et al., 2009. Broad neutralization of human immunodeficiency virus type 1 mediated by plasma antibodies against the gp41 membrane proximal external region. J. Virol. 83 (21), 11265.

Hammonds, J., et al., 2005. Induction of neutralizing antibodies against human immunodeficiency virus type 1 primary isolates by Gag-Env pseudovirion immunization. J. Virol. 79 (23), 14804.

Johnson, W.E., et al., 2003. Assorted mutations in the envelope gene of simian immunodeficiency virus lead to loss of neutralization resistance against antibodies representing a broad spectrum of specificities. J. Virol. 77 (18), 9993.

Keppler, O.T., et al., 2001. Susceptibility of rat-derived cells to replication by human immunodeficiency virus type 1. J. Virol. 75 (17), 8063.

Keppler, O.T., et al., 2002. Progress toward a human CD4/CCR5 transgenic rat model for de novo infection by human immunodeficiency virus type 1. J. Exp. Med. 195 (6), 719.

Kuhrt, D., et al., 2010. Evidence of early B-cell dysregulation in simian immunodeficiency virus infection: rapid depletion of naive and memory B-cell subsets with delayed reconstitution of the naive B-cell population. J. Virol. 84 (5), 2466–2476.

LaBranche, C.C., et al., 1995. A single amino acid change in the cytoplasmic domain of the simian immunodeficiency virus transmembrane molecule increases envelope glycoprotein expression on infected cells. J. Virol. 69 (9), 5217.

Li, Y., et al., 2007. Broad HIV-1 neutralization mediated by CD4-binding site antibodies. Nat. Med. 13 (9), 1032.

Mansfield, K., et al., 2008. Vaccine protection by live, attenuated simian immunodeficiency virus in the absence of high-titer antibody responses and high-frequency cellular immune responses measurable in the periphery. J. Virol. 82 (8), 4135.

Mattapallil, J.J., Letvin, N.L., Roederer, M., 2004. T-cell dynamics during acute SIV infection. AIDS 18 (1), 13.

Okada, H., et al., 2009. Synergistic effect of human CycT1 and CRM1 on HIV-1 propagation in rat T cells and macrophages. Retrovirology 6, 43.

Robinson, J.E., et al., 1998. Production and characterization of SIV envelope-specific rhesus monoclonal antibodies from a macaque asymptomatically infected with a live SIV vaccine. AIDS Res. Hum. Retroviruses 14 (14), 1253.
Rosati, M., et al., 2005. DNA vaccines expressing different forms of simian immunodeficiency virus antigens decrease viremia upon SIVmac251 challenge. J. Virol. 79 (13), 8480.
Sato, S., Johnson, W., 2007. Antibody-mediated neutralization and simian immunodeficiency virus models of HIV/AIDS. Curr. HIV Res. 5 (6), 594.
Scheid, J.F., et al., 2009a. Broad diversity of neutralizing antibodies isolated from memory B cells in HIV-infected individuals. Nature 458 (7238), 636.
Scheid, J.F., et al., 2009b. A method for identification of HIV gp140 binding memory B cells in human blood. J. Immunol. Methods 343 (2), 65.
Steger, K.K., et al., 1998. CD4+-T-cell and CD20+-B-cell changes predict rapid disease progression after simian-human immunodeficiency virus infection in macaques. J. Virol. 72 (2), 1600.
Yang, X., et al., 2000a. Modifications that stabilize human immunodeficiency virus envelope glycoprotein trimers in solution. J. Virol. 74 (10), 4746.
Yang, X., et al., 2000b. Characterization of stable, soluble trimers containing complete ectodomains of human immunodeficiency virus type 1 envelope glycoproteins. J. Virol. 74 (12), 5716.

MicroRNA Regulation of Glycoprotein B5R in Oncolytic Vaccinia Virus Reduces Viral Pathogenicity Without Impairing Its Antitumor Efficacy

Mina Hikichi[1], Minoru Kidokoro[2], Takeshi Haraguchi[3], Hideo Iba[3], Hisatoshi Shida[4], Hideaki Tahara[1,5] and Takafumi Nakamura[1,6]

[Q1] [1]*Core Facility for Therapeutic Vectors, Institute of Medical Science, Tokyo University, Tokyo, Japan;* [2]*Department of Virology III, National Institute of Infectious Diseases, Tokyo, Japan;* [3]*Division of Host-Parasite Interaction, Institute of Medical Science, Tokyo University, Tokyo, Japan;* [4]*Division of Molecular Virology, Institute for Genetic Medicine, Hokkaido University, Sapporo-shi, Japan;* [5]*Department of Surgery and Bioengineering Advanced Clinical Research Center, Institute of Medical Science, Tokyo University, Tokyo, Japan;* [6]*RNA and Biofunctions, Precursory Research for Embryonic Science and Technology (PRESTO), Japan Science and Technology Agency, Kawaguchi-shi, Japan*

Vaccinia virus, once widely used for smallpox vaccine, has recently been engineered and used as an oncolytic virus for cancer virotherapy. Their replication has been restricted to tumors by disrupting viral genes and complementing them with products that are found specifically in tumor cells. Here, we show that microRNA (miRNA) regulation also enables tumor-specific viral replication by altering the expression of a targeted viral gene. Since the deletion of viral glycoprotein B5R not only decreases viral pathogenicity but also impairs the oncolytic activity of vaccinia virus, we used miRNA-based gene regulation to suppress B5R expression through let-7a, a miRNA that is downregulated in many tumors. The expression of B5R and the replication of miRNA-regulated vaccinia virus (MRVV) with target sequences complementary to let-7a in the 3′-untranslated region (UTR) of the *B5R* gene depended on the endogenous expression level of let-7a in the infected cells. Intratumoral administration of MRVV in mice with human cancer xenografts that expressed low levels of let-7a resulted in tumor-specific viral replication and significant tumor regression without side effects, which were observed in the control virus. These results demonstrate that miRNA-based gene regulation is a potentially novel and versatile platform for engineering vaccinia viruses for cancer virotherapy.

Received 16 September 2010; accepted 7 February 2011; advance online publication 00 Month 2011. doi:10.1038/mt.2011.36

INTRODUCTION

Oncolytic viruses are promising therapeutic agents for cancer and are currently under preclinical and clinical investigation.[1] For example, vaccinia virus is a potential oncolytic virus because it has broad tropism in mammalian cells, a fast replication cycle, and no risk of integration into the host genome.[2] The replication cycle of vaccinia viruses only requires about 8 hours and results in cell lysis and release of progeny viruses. Furthermore, there is no risk of the viral genome integrating into the host genome because vaccinia viruses complete their entire life cycle in the cytoplasm, unlike most other DNA viruses. However, since viral toxicity is a potentially serious problem, the virus has been engineered to reduce its pathogenicity while retaining its oncolytic properties.[3,4]

The attenuated, replicating vaccinia virus strain LC16m8 is an attractive backbone for engineering a novel oncolytic agent because the strain has an extremely low neurovirulence profile.[5,6] In addition, LC16m8 has been safely administered to >100,000 infants and adults for smallpox vaccination and induced levels of immunity similar to those of the original Lister strain without serious side effects.[5,7,8] LC16m8 was isolated from LC16mO, which is a clone that was isolated from Lister strain through LC16, by repeated passages in primary rabbit kidney cells and selection for their temperature sensitivities.[5,6] As a result of attenuation, LC16m8 has a single nucleotide deletion in the open reading frame of the B5R gene.[9,10] B5R is a 42 kDa glycoprotein that is involved in virus [Q2] morphogenesis, trafficking, and dissemination.[11–19] Previously, the *B5R* gene was deleted from LC16m8 to develop a more genetically stable strain, LC16m8Δ.[20] In this study, we first compared the oncolytic potential of B5R-negative LC16m8Δ with B5R-positive LC16mO in mouse xenograft tumor model to determine the contribution of B5R to the pathogenicity and oncolytic potential of vaccinia virus.

Two strategies have been proposed to reduce the pathogenicity of vaccinia virus in normal cells and selectively target its oncolytic effects to tumor cells. In one strategy, insertional inactivation of vaccinia virus genes encoding thymidine kinase and/or epidermal growth factor-like vaccinia growth factor inhibits pathogenic viral replication in normal cells, while retaining its therapeutic replication in tumor cells that constitutively express thymidine kinase at high levels and have strong activation of the epidermal growth factor receptor pathway.[3,4] Thus, the success of this approach requires complementation of the disrupted viral genes by-products that are specifically found in tumor cells. Another strategy, transcriptional

Correspondence: *Takafumi Nakamura, Institute of Medical Science, Tokyo University, Minato-ku, Tokyo 108-8639, Japan. E-mail: taka@ims.u-tokyo.ac.jp*

targeting, uses tissue-specific promoters to restrict the replication of oncolytic viruses that have been developed from DNA viruses, such as adenovirus and herpes simplex virus, to malignant tissues.[21,22] However, this approach is not applicable to vaccinia viruses due to its cytoplasmic life cycle. As a result, an alternative strategy is needed to reduce the pathogenicity of vaccinia virus without impairing its oncolytic activity.

In this study, we used microRNA (miRNA)-based regulation of B5R to specifically target the oncolytic effects of vaccinia virus to tumor cells. Although this strategy has been applied to the development of oncolytic viruses from other DNA[23,24] and RNA[25,26] viruses, this is first application of the strategy to vaccinia virus. miRNAs are small noncoding RNAs (~22 nucleotides) that repress gene expression by binding to complementary sequences in the 3′-untranslated region (UTR) of messenger RNAs.[27,28] These post-transcriptional regulators play important roles in the control of tissue specification, tumorigenesis, and tumor progression. Since many miRNAs are differentially expressed in different tissues[29] and tumors,[30] they can be used to selectively promote viral replication in tumor cells expressing low levels of miRNA while inhibiting viral replication in normal cells that express higher levels of miRNA. An example of such a miRNA is let-7a, which belongs to the let-7 family of miRNAs that has lower expression in many kinds of cancer cells than in normal cells.[31–36] We successfully developed a miRNA-regulated vaccinia virus (MRVV) with let-7a miRNA complementary target sequences in the 3′UTR of *B5R*. This MRVV selectively replicates and induces oncolysis in tumor cells without toxicity in normal cells.

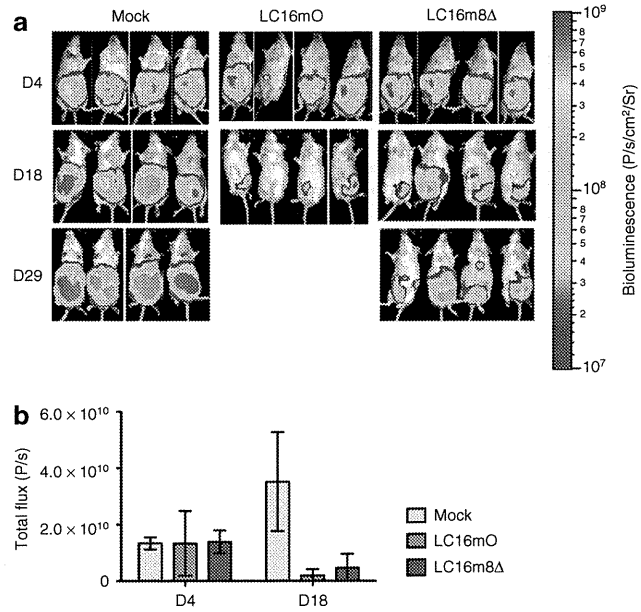

Figure 1 Comparison of the oncolytic effects of LC16m8Δ and LC16mO in mice bearing intraperitoneal xenografts. (**a**) BxPC-3 cells stably expressing luciferase (5 × 10^6 cells) were intraperitoneally injected into female severe combined immunodeficiency mice on day 0. Seven days after tumor implantation, the mice were intraperitoneally injected with a single dose of LC16mO or LC16m8Δ (1 × 10^7 plaque-forming unit/mouse). (**b**) *In vivo* tumor growth was monitored noninvasively by bioluminescence imaging after intraperitoneal administration of D-luciferin on days 4, 18, and 29. Quantification of the bioluminescence signals (photons/s) in the imaging data from days 4 and 18 in **a**. The data are presented as mean ± SD (n = 4).

RESULTS

Glycoprotein B5R is associated with viral pathogenicity and oncolytic activity

The *in vivo* oncolytic potentials of B5R-negative LC16m8Δ and B5R-positive LC16mO viruses in xenograft mouse model are compared in **Figure 1**. Four days after tumor implantation (day 4), the tumor growth in all of the implanted mice was similar. On day 18, tumor growth was significantly inhibited ($P < 0.001$) in both the LC16mO- and the LC16m8Δ-treated groups compared with the control group (**Figure 1a,b**). However, there was no significant difference in tumor volume reduction between the LC16mO- and LC16m8Δ-treated groups on this day (**Figure 1b**). In addition, all of the LC16mO-treated mice died or were sacrificed on days 21–28 because they exhibited symptoms of severe viral toxicity, such as weight loss and pock lesions on their tail, paws, face, and other areas of the body surface (data not shown). Although LC16m8Δ-treated mice did not show these symptoms, tumor regrowth was observed after day 29 (**Figure 1a**).

A schematic representation of the restoration of *B5R* in recombinant vaccinia virus LC16m8Δ-B5R is shown in **Figure 2a**. LC16m8Δ lysed A549, BxPC-3, Caco-2, and HeLa cells more efficiently than HEp-2, MDA-MB-231, PANC-1, and SK-N-AS cells. Although the cytolytic activity of LC16m8Δ was much lower than that of LC16mO in all tumors, B5R expression fully restored its oncolytic activity (**Figure 2b**).

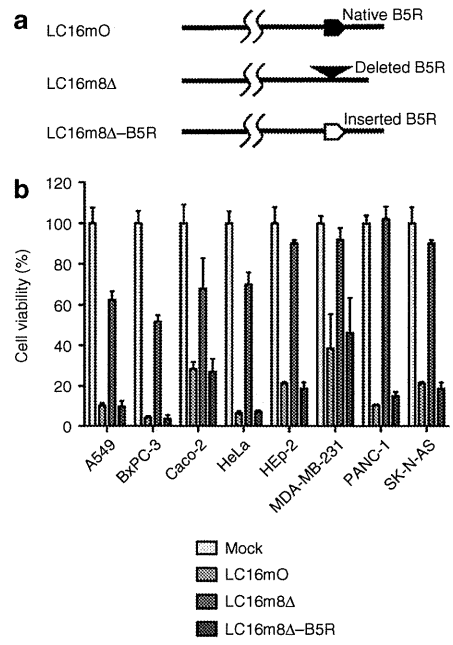

Figure 2 Relationship between B5R expression and oncolytic activity. (**a**) Schematic representation of the recombinant vaccinia virus LC16m8Δ-B5R. (**b**) Human cell lines were infected with B5R-positive or B5R-negative viruses at a multiplicity of infection of 0.5. The cell viabilities were determined 120 hours postinfection and are expressed as percentages of the cell survival of mock-infected cultures. The data are presented as mean + SD (n = 3).

B5R expression and the replication of miRNA-regulated vaccinia virus are dependent on endogenous let-7a

A schematic representation of MRVV with B5R-EGFP (BG) fusion protein (MRVV/BG) is shown in **Figure 3a**. The expression level of mature let-7a miRNA in normal human lung fibroblasts (NHLF) cells was three to four times higher than that in human lung and pancreatic carcinoma cell lines A549, BxPC-3, and PANC-1. On the other hand, there was less than a twofold difference in let-7a expression between NHLF and cervical carcinoma cell line HeLa (**Figure 3b**). These expression levels of let-7a correlate with functional activities of let-7a as measured by luciferase reporter assay. As shown in **Figure 3c**, the presence of four copies of let-7a target sequences in the 3′UTR of firefly luciferase (*FLuc*) mRNA in HeLa cells resulted in >96% of suppression of *FLuc* expression compared with the presence of four copies of the disrupted target sequences. In contrast, the suppression of *FLuc* expression in A549 and BxPC-3 cells was much weaker than that in HeLa cells. Thus, HeLa cells have five to seven times more let-7a activity than A549 and BxPC-3 cells (**Figure 3c**).

During infection of HeLa and NHLF cells, LC16m8Δ-B5Rgfp$_{let7a}$ did not induce a cytopathic effect (CPE) with B5R-enhanced green fluorescent protein (EGFP) expression, whereas LC16mO and the control viruses LC16m8Δ-B5Rgfp (lacking miRNA target sequences) and LC16m8Δ-B5Rgfp$_{let7a\text{-}mut}$ (containing the disrupted miRNA target sequences) resulted in a massive CPE after B5R-EGFP expression (**Figure 3d**). Simultaneously, the replication of LC16m8Δ-B5Rgfp$_{let7a}$ replication in HeLa and NHLF cells, which was equivalent to that of LC16m8Δ, was reduced by two log orders compared with that of LC16mO, LC16m8Δ-B5Rgfp, and LC16m8Δ-B5Rgfp$_{let7a\text{-}mut}$

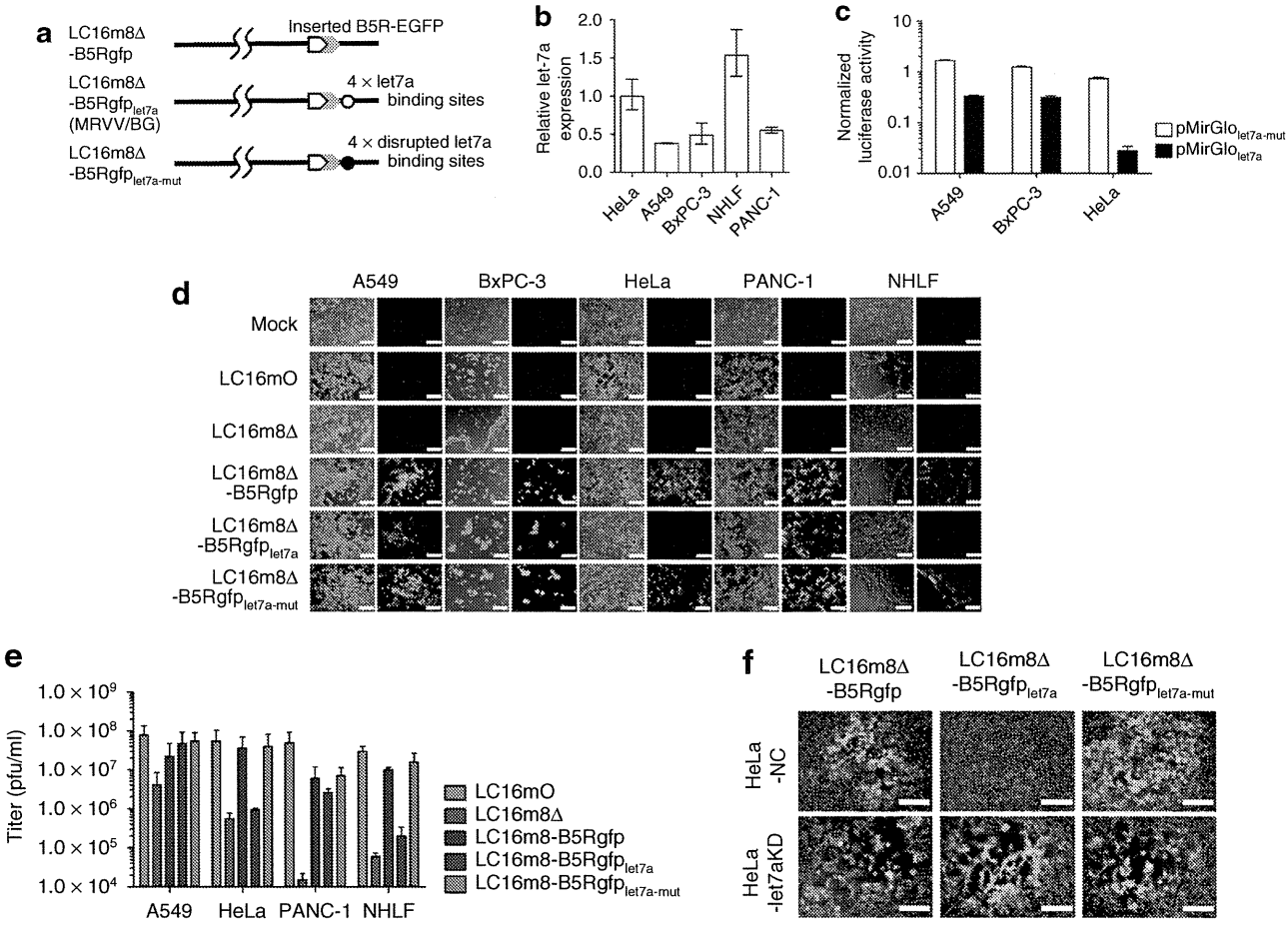

Figure 3 Construction and characterization of recombinant microRNA (miRNA)-regulated vaccinia virus (MRVV). (**a**) Schematic representation of the recombinant vaccinia virus genome showing the modified B5R protein fused with enhanced green fluorescent protein at its C-terminus (MRVV/BG). Four copies of let-7a miRNA complementary or disrupted target sequences, flanked by *NheI*/*AgeI* restriction sites, were incorporated into the 3′-untranslated region of the *B5R* gene. (**b**) Relative expression of mature let-7a miRNA in the indicated cell lines by real-time PCR analysis. The data are the let-7a level normalized with the U6 small nuclear RNA level relative to that in HeLa cells and are represented by the mean ± SD (n = 3). (**c**) The cell lines expressing different levels of let-7a were transfected with pMirGlo$_{let7a\text{-}mut}$ or pMirGlo$_{let7a}$ plasmid containing two expression units encoding firefly luciferase (*FLuc*) used as the primary reporter to monitor mRNA regulation and Renilla luciferase (*RLuc*) acting as a transfection control. Dual luciferase assay was performed 24 hours post-transfection. The *FLuc* activity is normalized to the *RLuc* activity. The data are presented as mean + SD (n = 3). (**d**) The cell lines expressing different levels of let-7a were infected with the MRVV/BG at an multiplicity of infection (MOI) of 0.1 and photographed using phase-contrast or fluorescence microscopy of the same field 3 days later. Bar = 200 μm. (**e**) One-step growth of the MRVV/BG was determined by titration of the viruses that were collected from the infected cells shown in **(d)**. The data are presented as mean + SD (n = 3). (**f**) HeLa-let7aKD cells (let-7a miRNA knockdown) or HeLa-NC cells (negative control) were infected with the MRVV/BG at an MOI of 0.1 and photographed 3 days later. The combined phase-contrast and fluorescence images are shown. Bar = 200 μm.

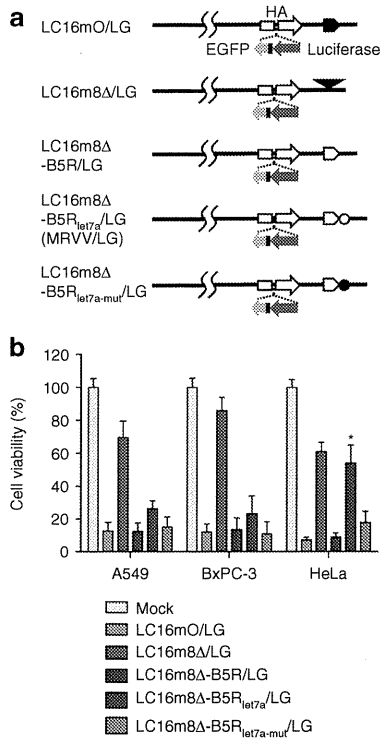

Figure 4 Effect of transgene insertion into microRNA (miRNA)-regulated vaccinia virus (MRVV) on its oncolytic activity *in vitro*. (**a**) Schematic representation of the recombinant vaccinia virus genome with the expression cassette that encodes both luciferase and enhanced green fluorescent protein reporters miRNA-regulated vaccinia virus (MRVV) luciferase (L) and enhanced green fluorescent protein (G) reporters (MRVV/LG). The symbols are the same as those used in **Figures 2a** and **3a**. (**b**) The cell viability after infection with MRVV/LG was determined as described in **Figure 2b**. The data are presented as mean + SD ($n = 3$). *$P < 0.001$ for LC16m8Δ-B5R$_{let7a}$/LG versus LC16m8Δ-B5R$_{let7a-mut}$/LG in HeLa cells.

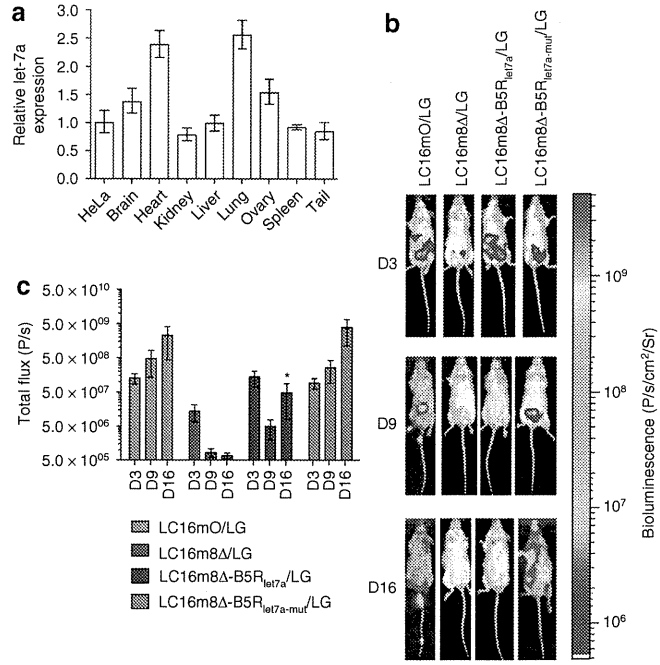

Figure 5 Biodistribution and replication of microRNA (miRNA)-regulated vaccinia virus (MRVV) luciferase (L) and enhanced green fluorescent protein (G) reporters (MRVV/LG) *in vivo*. (**a**) Relative expression of mature let-7a miRNA in the indicated mouse normal tissues by real-time PCR analysis. The data are the let-7a level normalized with the U6 small nuclear RNA level relative to that in HeLa cells and are represented by the mean ± SD ($n = 3$). (**b**) Representative images of the biodistribution of MRVV/LG in severe combined immunodeficiency mice that were intraperitoneally injected with 1×10^7 plaque-forming unit of MRVV/LG ($n = 3$). The biodistributions were visualized by intraperitoneal injection of D-luciferin at 3, 9, and 16 days after viral administration. The vaccinia virus designations are the same as those used in **Figure 4a**. (**c**) Quantitation of the bioluminescence signals in photons/s, calculated from the imaging data in **(b)**. The data are presented as mean ± SD ($n = 3$). *$P < 0.001$ for LC16m8Δ-B5R$_{let7a}$/LG versus LC16m8Δ-B5R$_{let7a-mut}$/LG on day 16.

(**Figure 3e**). In contrast, there were no differences in the CPE and replication in A549, BxPC-3, and PANC-1 cells among LC16m8Δ-B5Rgfp, LC16m8Δ-B5Rgfp$_{let7a}$, and LC16m8Δ-B5Rgfp$_{let7a-mut}$ (**Figure 3d,e**). Furthermore, the CPE and replication of LC16m8Δ-B5Rgfp, LC16m8Δ-B5Rgfp$_{let7a}$, and LC16m8Δ-B5Rgfp$_{let7a-mut}$ in A549, BxPC-3, and PANC-1 cells were comparable with those of LC16mO but were much greater than those of LC16m8Δ (**Figure 3d,e**). In addition, the presence of miRNA-based gene regulation was confirmed by using HeLa-let7aKD cells where TuD RNA largely suppresses endogenous let-7a activity (**Supplementary Figure S1**). LC16m8Δ-B5Rgfp$_{let7a}$ induced a CPE after B5R-EGFP expression in HeLa-let7aKD cells but not in HeLa-NC cells, although LC16m8Δ-B5Rgfp and LC16m8Δ-B5Rgfp$_{let7a-mut}$ showed a massive CPE after B5R-EGFP expression in both cell types (**Figure 3f**). Collectively, these results clearly demonstrate that B5R expression and the replication of LC16m8Δ-B5Rgfp$_{let7a}$ were regulated by endogenous let-7a.

Transgene insertion into microRNA-regulated vaccinia virus does not affect let-7a miRNA-regulated oncolytic activity

A schematic representation of MRVV with luciferase (L) and EGFP (G) reporters (MRVV/LG) is shown in **Figure 4a**. Although LC16m8Δ-B5R$_{let7a}$/LG lysed A549 and BxPC-3 cells with low levels of let-7a more efficiently than LC16m8Δ/LG, there was no significant difference in the oncolytic activities of LC16m8Δ-B5R$_{let7a}$/LG and LC16m8Δ/LG against HeLa cells with higher levels of let-7a (**Figure 4b**). In addition, the oncolytic activity of LC16m8Δ-B5R$_{let7a}$/LG was significantly lower than that of LC16m8Δ-B5R$_{let7a-mut}$/LG in HeLa cells; however, there was no significant difference in their oncolytic activities in A549 and BxPC-3 cells. Finally, LC16mO/LG, LC16m8Δ-B5R/LG, and LC16m8Δ-B5R$_{let7a-mut}$/LG showed a similar oncolytic effect against A549, BxPC-3, and HeLa cells. These results indicated that transgene insertion into the vaccinia virus genome did not affect let-7a miRNA-regulated oncolytic activity.

miRNA-based regulation of vaccinia virus inhibits viral replication in normal tissues

It has been reported that let-7a is highly conserved in humans and mice and is ubiquitous and abundant in normal tissues.[27,37,38] Similarly, we confirmed ubiquitous let-7a RNA accumulation in all mouse tissues tested (**Figure 5a**). Real-time PCR analysis showed that the brain, heart, lung, and ovary have higher expression level of let-7a than HeLa cells do, while the kidney, liver, spleen, and

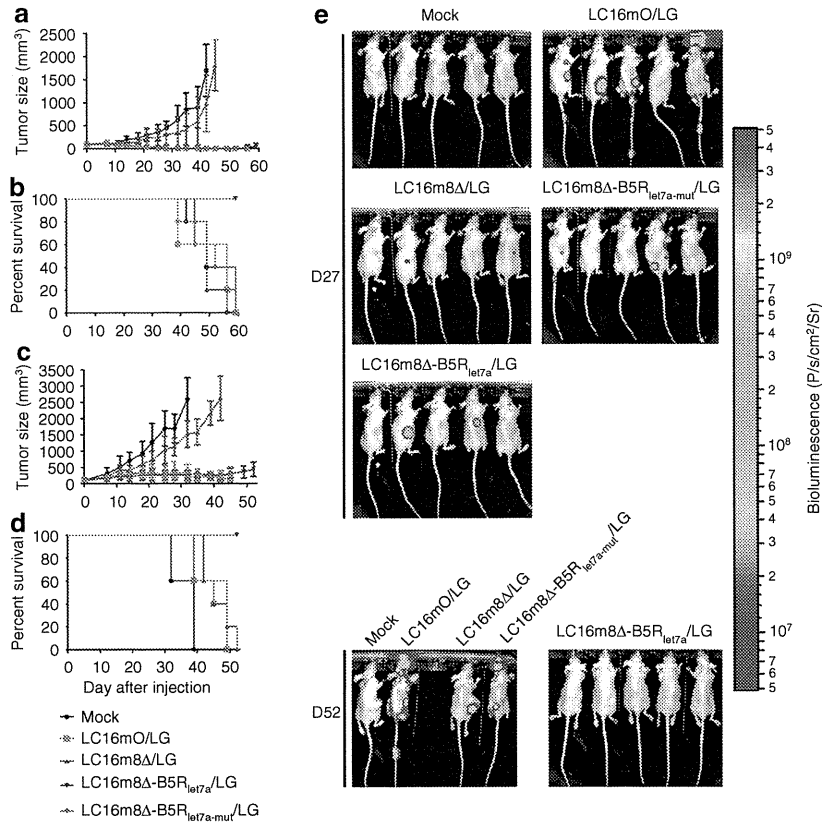

Figure 6 MicroRNA (miRNA)-regulated vaccinia virus (MRVV) luciferase (L) and enhanced green fluorescent protein (G) reporters (MRVV/LG) reduces viral pathogenicity while maintaining oncolytic activity *in vivo*. (**a**,**c**) Nude mice bearing established subcutaneous (**a**) BxPC-3 tumors or (**c**) A549 tumors were treated with intratumoral injections of MRVV/LG [1 × 10^7 plaque-forming unit (pfu)/injection, 3 × 10^7 pfu/mouse] on days 0, 3, and 6. The vaccinia virus designations are the same as those used in **Figure 4a**. The data are presented as mean ± SD (n = 5). (**b**,**d**) Survival curves of the mice that are shown in **a** and **c**. (**e**) *In vivo* biodistribution of MRVV/LG, determined by noninvasive imaging after intraperitoneal injection of D-luciferin into the mice that are shown in **(a, b)** on days 27 and 52.

tail have let-7a expression comparable to HeLa cells. Therefore, *in vivo* let-7a regulation was evaluated by a single intraperitoneal injection of each virus and noninvasive bioluminescence imaging in severe combined immunodeficiency (SCID) mice. Three days after injection of LC16mO/LG, LC16m8Δ/LG, LC16m8Δ-B5R$_{let7a}$/LG, or LC16m8Δ-B5R$_{let7a-mut}$/LG into SCID mice (day 3), the biodistribution of these viruses was concentrated in the abdomen. On days 9 and 16, the LC16mO/LG and LC16m8Δ-B5R$_{let7a-mut}$/LG viruses spread to several areas of their body, including the tail, paws, and face, where pock lesions were observed; however, the LC16m8Δ/LG and LC16m8Δ-B5R$_{let7a}$/LG viruses did not spread much (**Figure 5b**). In addition, there were significant differences in transgene expression levels and replication between LC16m8Δ-B5R$_{let7a}$/LG (or LC16m8Δ-/LG) and LC16m8Δ-B5R$_{let7a-mut}$/LG (or LC16mO/LG) on day 16 but not on days 3 and 9 (**Figure 5c**). To clear the relationship between B5R expression and the replication of MRVV in normal tissues, LC16m8Δ-B5Rgfp, LC16m8Δ-B5Rgfp$_{let7a}$, or LC16m8Δ-B5Rgfp$_{let7a-mut}$ was intraperitoneally injected into SCID mice, and the virus-associated B5R-EGFP expression was examined 15 days after injection. As expected, LC16m8Δ-B5Rgfp and LC16m8Δ-B5Rgfp$_{let7a-mut}$ caused pock lesions on the tail, where B5R-EGFP expression was detected. In contrast, no pock lesion and B5R-EGFP expression were observed on the tail of LC16m8Δ-B5Rgfp$_{let7a}$-injected mice (**Supplementary Figure S2**). Taken together, these results demonstrate that let-7a miRNA-based regulation inhibits vaccinia virus replication in normal cells by downregulating B5R in cells infected with MRVV.

miRNA-regulated vaccinia virus reduces viral pathogenicity while maintaining oncolytic activity after tumor-specific replication in mouse tumor models

LC16m8Δ-B5R$_{let7a}$/LG induced a significantly stronger antitumor effect than LC16m8Δ/LG in nude mice with subcutaneous BxPC-3 tumors (P < 0.001 on days 39–45; **Figure 6a**) or A549 tumors (P < 0.001 on days 25–42; **Figure 6c**) without the severe viral toxicity associated with LC16mO/LG and LC16m8Δ-B5R$_{let7a-mut}$/LG. Furthermore, in the BxPC-3 model, four out of five LC16m8Δ-B5R$_{let7a}$/LG-treated mice showed complete tumor regression without any symptoms of toxicity at the end of the experiment. Similarly, in the A549 model, the LC16m8Δ-B5R$_{let7a}$/LG-treated mice showed reduced tumor growth but not complete tumor regression. Although the degree of tumor regression in the LC16mO/LG- and LC16m8Δ-B5R$_{let7a-mut}$/LG-treated mice was similar to that of the LC16m8Δ-B5R$_{let7a}$/LG-treated mice in both tumor models, all of the mice treated with the former viruses died or were sacrificed on days 39–59 due to severe viral toxicity, such as pock lesions and weight loss. Finally, all of the mock- or

LC16m8Δ-treated mice were sacrificed by the end of the experiment due to their great tumor burden. Thus, infection with the LC16m8Δ-B5R$_{let7a}$/LG virus resulted in a significantly longer survival than infection with any of the other viruses in both mouse xenograft models ($P < 0.005$; **Figure 6b,d**).

These results were confirmed by bioluminescence imaging, which showed tumor-specific replication of LC16m8Δ-B5R$_{let7a}$/LG in BxPC-3 xenografts (**Figure 6e**) and A549 xenografts (**Supplementary Figure S3**). Three and 10 days after intratumoral injection of LC16mO/LG, LC16m8Δ/LG, LC16m8Δ-B5R$_{let7a}$/LG, or LC16m8Δ-B5R$_{let7a\text{-}mut}$/LG (days 3 and 10), the biodistribution of these viruses was concentrated in the tumor in nude mice bearing BxPC-3 (data not shown) or A549 xenografts (**Supplementary Figure S3**). On day 20, the LC16mO/LG and LC16m8Δ-B5R$_{let7a\text{-}mut}$/LG viruses spread to several areas of their body, including the tail, paws, and face, where pock lesions were observed; however, the LC16m8Δ/LG and LC16m8Δ-B5R$_{let7a}$/LG viruses did not spread (**Supplementary Figure S3**). On day 27, there was no viral replication in three of the tumor-free mice treated with LC16m8Δ-B5R$_{let7a}$/LG, whereas two of the mice with reduced tumor growth still showed tumor-specific viral replication (**Figure 6e**). On day 52, no viral replication was observed in normal tissues after the tumor had regressed completely in all five mice. In contrast, on day 27, viruses had already spread from tumor to normal tissues even in the tumor-free mice treated with LC16mO/LG and LC16m8Δ-B5R$_{let7a\text{-}mut}$/LG. By day 52, all of the surviving mice had widespread viruses in their tail, paws, ears, and face (**Figure 6e**). Finally, LC16m8Δ/LG replication was tumor-specific; however, it was much slower than that of the other viruses, which resulted in weaker oncolytic activity (**Figure 6e** and **Supplementary Figure S3**).

DISCUSSION

The viral glycoprotein B5R plays important roles in packaging intracellular matured virions with membranes derived from the trans-Golgi network or early endosomes to form intracellular enveloped virions.[12,16,17] Intracellular enveloped virions are transported along microtubules to the cell periphery[15,18] where they adhere to the cell surface as a cell-associated enveloped virions. B5R, along with the A36R and A33R proteins, is also involved in the Src kinase-dependent process of forming actin-containing microvilli and releasing cell-associated enveloped virions from the cell surface to form extracellular enveloped virions (EEVs).[13,14] Since EEVs are critical for cell-to-cell and long-range virus spreading, B5R dysfunction markedly reduces the formation of EEVs and results in small viral plaques *in vitro* and highly attenuated viruses *in vivo*.[10,11,17,19,20]

In addition, this study demonstrated that the deletion of B5R weakens its oncolytic activity, as shown by the reduced antitumor efficacy of B5R-negative LC16m8Δ in mouse xenograft tumor models (**Figures 1a** and **6a,c**). These results were confirmed by replication of LC16m8Δ *in vivo*, which was not only spatially restricted within the injected tumor but also slower replicating than B5R-positive viruses (**Figure 6e** and **Supplementary Figure S3**). The EEV is also surrounded by a host cell-derived envelope that contains several host complement control proteins and a few exposed viral proteins.[39–41] Among these proteins, B5R is the only target for EEV-neutralizing antibodies.[39] Nevertheless, high EEV-producing strains of vaccinia virus spread between tumors more efficiently than low EEV-producing strains, even in the presence of EEV-neutralizing antibodies, in a syngeneic mouse tumor model.[42] Collectively, these results suggest that strategies that regulate the expression of B5R, such as miRNA, are promising approaches for engineering safe and effective vaccinia viruses for cancer virotherapy.

Recently, tumor-targeting approaches using miRNA have been used to develop oncolytic viruses based on adenovirus,[23] coxsackievirus A21,[26] herpes simplex virus 1,[24] and vesicular stomatitis virus.[25] The tumor-specific replication of these engineered viruses has decreased their pathogenic effects in normal tissues. For example, the insertion of miRNA target sequences for muscle-specific miRNA into coxsackievirus A21 decreased myositis without compromising antitumor activity.[26] Similarly, insertion of miRNA target sequences for hepatocyte-specific miRNA into adenovirus reduced hepatotoxicity.[23] Since vaccinia virus exhibits broad host cell tropism, we used tumor-suppressed miRNA rather than tissue-specific miRNA to develop the MRVV. In addition, we selected let-7a miRNA because the let-7 family of miRNAs is highly conserved and abundantly expressed in many types of normal cells.[27,38] However, the expression of let-7a is downregulated in tumor cells isolated from patients with breast,[31] hepatocellular,[32] lung,[33,34] melanoma,[35] and pancreatic[36] carcinomas.

For example, let-7a is reportedly expressed in ~50% of tumor cell lines and tumor tissues from patients with lung or pancreatic cancer at <20% of the expression in normal cells and tissues adjacent to the tumors.[33,36] Similarly, the expression of let-7a in the human A549 lung, BxPC-3 pancreatic, and HeLa cervical carcinoma cell lines used in this study was reduced by ~25, 30, and 65% of the expression in NHLF, respectively (**Figure 3b**). Remarkably, the HeLa cells have five to seven times more let-7a activity than the A549 and BxPC-3 cells despite an approximately twofold difference of let-7a expression between these cells (**Figure 3c**). Considering that it has been proposed that target suppression depends on a threshold miRNA concentration,[43] the concentration of let-7a in HeLa cells may be sufficient to reach the threshold expression level necessary for strong suppression. On the other hand, perfectly complementary target sites for let-7a of MRVV may be subject to regulation by all the other members of the let-7 family that are expressed in HeLa cells as described previously.[43] Anyhow, B5R expression and the replication of MRVV/BG were almost completely inhibited by let-7a miRNA-based regulation in not only the NHLF but also HeLa cells (**Figure 3d–f**). Furthermore, B5R-EGFP expression and the replication of MRVV/BG were also abrogated on the mouse tail that has let-7a expression comparable to HeLa cells (**Figure 5a** and **Supplementary Figure S2**). Our findings are consistent with previous reports concerning let-7a miRNA-based regulation of vesicular stomatitis viral[25] and polioviral[37] replication in HeLa cells and mouse models. In contrast, the expression of let-7a in the A549, BxPC-3, and PANC-1 cells was low enough to induce efficient replication of MRVV/BG in these tumor cells and xenografts, although the residual let-7a activity slightly repressed the B5R expression of MRVV/BG *in vitro* (**Figure 3d**) and *in vivo* (**Supplementary Figure S4**).

In a rare example, Kelly *et al.* showed that oncolytic coxsackie virus A21 with inserted muscle-specific miRNA target sequences escaped from the cellular miRNA system by mutation of the target inserts.[26] We did not find any indication of escaped mutants from LC16m8Δ-B5R$_{let7a}$/LG, as shown in the bioluminescence images of the BxPC-3 model (**Figure 6e**). Furthermore, sequence analysis did not show any mutations in the target inserts of LC16m8Δ-B5R$_{let7a}$/LG or LC16m8Δ-B5Rgfp$_{let7a}$ during cell culture passages. As reported previously,[20] B5R^{+} revertants spontaneously emerged from LC16m8 by frameshift mutation resulting from a single nucleotide insertion at site just upstream of the deletion site in the open reading frame of the *B5R* gene. Since the MRVV has four copies of miRNA complementary target sequences for let-7a in the 3′UTR (and not the open reading frame) of the *B5R* gene, it is unlikely that a slight mutation would result in a significantly different phenotype, even if a mutation in these target inserts occurred during viral replication.

On the other hand, the spread of LC16m8Δ-B5R$_{let7a}$/LG was much less than that of the unregulated LC16mO/LG or the control LC16m8Δ-B5R$_{let7a\text{-}mut}$/LG in SCID mice and therefore did not cause any pock lesions in normal mouse tissues where let-7a is abundant (**Figure 5a–c**). However, quantitation of the bioluminescence signal from the luciferase-expressing vaccinia revealed that the LC16m8Δ-B5R$_{let7a}$/LG signal was still higher by 1–2 log orders than the B5R-deleted LC16m8Δ/LG signal (**Figure 5c**). These results suggest that miRNA-mediated inhibition of B5R expression may be overcome by miRNA saturation, which has been observed by Kelly *et al.* previously.[44] The possibility is also supported by another data that no B5R-EGFP expression was observed in HeLa cells infected with LC16m8Δ-B5Rgfp$_{let7a}$ at an multiplicity of infection (MOI) of 0.1 (**Figure 3d**); however, 100-fold higher input multiplicities of LC16m8Δ-B5Rgfp$_{let7a}$ allowed B5R-EGFP expression in HeLa cells (data not shown). Thus, more attention should be paid to miRNA saturation rather than to mutation of miRNA target inserts in designing vaccinia viruses for future use. In this regard, incorporation of different miRNA target sequences of more than one miRNA species might be one strategy to address the question of miRNA saturation.

In conclusion, we developed a highly attenuated MRVV with let-7a miRNA complementary target sequences in the 3′UTR of the *B5R* gene. This MRVV could selectively replicate and induce oncolysis in tumor cells without affecting normal cells, depending on the miRNA expression level. More generally, this study shows that control of viral replication and oncolytic activity by miRNA-based gene regulation provides a potentially novel and versatile platform for engineering vaccinia viruses for cancer virotherapy.

MATERIALS AND METHODS

Plasmid construction. The construction of all plasmids used in this study is described in the **Supplementary Materials and Methods.**

Cell culture. Human carcinoma cell lines [lung A549 (Ham's F12K); pancreatic BxPC-3, PANC-1 and neuroblastoma SK-N-AS (RPMI-1640); colorectal Caco-2, epidermoid HEp-2 (E-MEM); cervical HeLa and breast MDA-MB-231 (D-MEM)] and rabbit kidney-derived RK13 cells (E-MEM) were obtained from the American Type Culture Collection [Q4][Q5] (Manassas, VA) and grown in their respective mediums (Wako, Richmond, VA) with 10% fetal bovine serum (Hyclone, Waltham, MA) at 37 °C in a humidified atmosphere with 5% CO_2. NHLF cells was purchased from TaKaRa Biomedicals and cultured according to the manufacturer's protocol. [Q6] HeLa-let7aKD or HeLa-NC cells were generated by infecting HeLa cells with lentivirus expressing tough decoy (TuD) RNA against let-7a or a negative control, respectively, with the human 7SK RNA polymerase III promoter,[45] as described previously.[46] Single HeLa-let7aKD or HeLa-NC cell isolates were expanded and selected in media containing 5 μg/ml puromycin (Sigma, St Louis, MO). [Q7]

Virus construction. To construct viruses with B5R, namely, LC16m8Δ-B5R and LC16m8Δ-B5Rgfp, RK13 cells were infected with B5R-deleted LC16m8Δ viruses[20] at a MOI of 0.02, and then transfected with pB5R or pTN-B5Rgfp. After harvesting the progeny viruses 2–5 days later, LC16m8Δ-B5R and LC16m8Δ-B5Rgfp were selected on the basis of larger plaque size and/or enhanced EGFP expression, by three serial plaque purifications. Finally, the insertion of *B5R* was verified by sequencing the modified region.

Similarly, miRNA-regulated viruses, namely, LC16m8Δ-B5R$_{let7a}$, LC16m8Δ-B5R$_{let7a\text{-}mut}$, LC16m8Δ-B5Rgfp$_{let7a}$, and LC16m8Δ-B5Rgfp$_{let7a\text{-}mut}$ were constructed by infecting RK13 cells with LC16m8Δ viruses, as described above, and then transfecting them with pTN-B5R$_{let7a}$ × 4, pTN-B5R$_{let7a\text{-}mut}$ × 4, pTN-B5Rgfp$_{let7a}$ × 4, or pTN-B5Rgfp$_{let7a\text{-}mut}$ × 4, respectively.

Likewise, the viruses expressing luciferase and EGFP, namely, LC16mO/LG, LC16m8Δ/LG, LC16m8Δ-B5R/LG, LC16m8Δ-B5R$_{let7a}$/LG, and LC16m8Δ-B5R$_{let7a\text{-}mut}$/LG, were constructed by infecting RK13 cells with LC16mO, LC16m8Δ, LC16m8Δ-B5R, LC16m8Δ-B5R$_{let7a}$, or LC16m8Δ-B5R$_{let7a\text{-}mut}$ viruses, respectively, as described above, and then transfecting them with pSFJvnc110-LucIRESgfp. All viruses were propagated and titrated in RK13 cells and stored at −80 °C.

Quantification of let-7a miRNA. First, total RNA was isolated from A549, BxPC-3, HeLa, PANC-1, and NHLF cells and also normal brain, heart, kidney, liver, lung, ovary, spleen, and tail of 6-week-old female athymic nude mice (Charles River Laboratories, Yokohama, Japan) using the [Q8] mirVana microRNA isolation kit (Ambion, Carlsbad, CA). Then, expres- [Q9] sion of mature let-7a miRNA and the endogenous control were quantified by real-time PCR using the TaqMan microRNA assay kit (Applied Biosystems, Carlsbad, CA) for has-let-7a miRNA and U6 small nuclear [Q10] RNA (snRNA), respectively. The relative expression of let-7a was calculated by using the comparative threshold method (Applied Biosystems User Bulletin No. 2).

Luciferase reporter assay. Cells in 96-well optical-bottom white plates (Nunc, Rochester, NY) were transfected with 0.1 μg of pMirGlo$_{let7a}$ or [Q11] pMirGlo$_{let7a\text{-}mut}$ plasmid containing two expression units that encode Renilla luciferase (*RLuc*) acting as a transfection control and *FLuc* with four copies of let-7a target sequences or the disrupted sequences in the 3′UTR respectively, using Fugene HD (Roche, Basel, Switzerland). At 24 [Q12] hours after transfection, the cells were analyzed for luciferase activities using the Dual-Glo Luciferase Assay System (Promega, Madison, WI). [Q13]

Viral infection. Each cell line was infected with a vaccinia virus at an MOI of 0.1 or 0.5 plaque-forming unit (pfu)/cell, respectively, in Opti-MEM medium (Invitrogen, Carlsbad, CA) for 1 hour at 37 °C in 24-well or [Q14] 96-well plates. Seventy-two hours after infection, the cells in the 24-well plate were photographed under phase-contrast or fluorescence microscopy. Subsequently, the infected cells were harvested into 1 ml of growth medium and sonicated to release the replicated viruses for titration in RK13 cells. One hundred twenty hours after infection, the viability of the cells in the 96-well plate was determined by using the CellTiter 96 AQueous cell proliferation assay kit (Promega).

In vivo *experiments.* The protocols for the following animal experiments were approved by the Animal Experiment Committee of the Institute of Medical Science, University of Tokyo, Japan.

In the first *in vivo* experiment, BxPC-3 cells stably expressing luciferase (5×10^6 cells in 100 µl of phosphate-buffered saline, pH 7.4) were intraperitoneally injected into 6-week-old female SCID mice (Charles River Laboratories) on day 0. Seven days later, the mice were administered a single intraperitoneal injection of LC16mO or LC16m8Δ (1×10^7 pfu in 100 µl of Opti-MEM per mouse). Control animals (mock therapy) were injected with 100 µl of Opti-MEM without any virus. To monitor *in vivo* tumor growth noninvasively, 150 µl of D-luciferin (15 mg/ml) was administered to the treated mice on days 4, 18, and 29. The mice were anesthetized with isoflurane before imaging the tumors with the IVIS [Q15] 100 bioluminescence imaging system (Xenogen, Hopkinton, MA). The bioluminescence signals were quantified according to the manufacturer's protocol.

In the second *in vivo* experiment, 6-week-old female SCID mice were intraperitoneally injected with a single dose of each vaccinia virus expressing luciferase (1×10^7 pfu in 100 µl of Opti-MEM per mouse) on day 0. To monitor the *in vivo* viral growth, D-luciferin was injected into the mice on days 3, 9, or 16, and then they were examined by bioluminescence imaging, as described above.

In the third *in vivo* experiment, subcutaneous tumors were established by injecting A549 or BxPC-3 cells (5×10^6 cells in 100 µl of phosphate-buffered saline, pH 7.4) into the right flank of 6-week-old female athymic nude mice (Charles River Laboratories). When the tumors reached 5–8 mm in diameter, the mice received three intratumoral injections of each vaccinia virus (1×10^7 pfu in 100 µl of Opti-MEM per mouse) on days 0, 3, and 6. Control animals (mock therapy) were injected with 100 µl of Opti-MEM without any virus. The mice were euthanized at the end of the experiment or when any of the following occurred: tumor burden exceeded 2,500 mm^3, tumor ulceration occurred, or symptoms of severe viral toxicity, such as pock lesions on body surfaces and weight loss of >30%, manifested. The diameter of tumors was measured three times per week, and the volume of a tumor was calculated according to the formula: volume = $0.5 \times \text{length} \times \text{width}^2$. The virus biodistribution was determined by injecting D-luciferin into the mice on day 27 or 52, followed by bioluminescence imaging, as described above.

Statistical analysis. The differences in cytolytic activity, *in vivo* viral replication, and tumor burden between treatment groups were analyzed for statistical significance by one-way or two-way ANOVA and the Bonferroni test when ANOVA showed overall significance. P values <0.05 were considered to be statistically significant. Survival curves were constructed using the Kaplan–Meier method. Survival times were statistically analyzed by using the log-rank test. Data were analyzed using GraphPad Prism Ver 5 (GraphPad Software).

SUPPLEMENTARY MATERIAL

Figure S1. Inhibitory effects of TuD RNA on endogenous let-7a activity.

Figure S2. B5R expression of miRNA-regulated vaccinia virus in normal tissues.

Figure S3. Representative images of the biodistribution of MRVV/LG, determined by noninvasive imaging after intraperitoneal injection of D-luciferin into the mice that are shown in (**Figure 6c,d**) on days 3, 10, and 20.

Figure S4. B5R expression of miRNA-regulated vaccinia virus in subcutaneous mouse xenografts that expressed low levels of let-7a.

Materials and Methods.

ACKNOWLEDGMENTS

This work was supported by the Precursory Research for Embryonic Science and Technology (PRESTO) program in RNA and Biofunctions from the Japan Science and Technology Agency and partly supported by a Grant-in-Aid for Young Scientists (A) from the Ministry of Education, Culture, Sports, Science and Technology of Japan (to T.N.).

REFERENCES

1. Parato, KA, Senger, D, Forsyth, PA and Bell, JC (2005). Recent progress in the battle between oncolytic viruses and tumours. *Nat Rev Cancer* **5**: 965–976.
2. Moss, B (2001). Poxviridae: The viruses and their replication. In: Knipe, DM, Howley, PM eds. *Fields Virology*. Lippincott: Philadelphia, PA, pp 2849–2883.
3. Park, BH, Hwang, T, Liu, TC, Sze, DY, Kim, JS, Kwon, HC *et al.* (2008). Use of a targeted oncolytic poxvirus, JX-594, in patients with refractory primary or metastatic liver cancer: a phase I trial. *Lancet Oncol* **9**: 533–542.
4. Zhang, Q, Yu, YA, Wang, E, Chen, N, Danner, RL, Munson, PJ *et al.* (2007). Eradication of solid human breast tumors in nude mice with an intravenously injected light-emitting oncolytic vaccinia virus. *Cancer Res* **67**: 10038–10046.
5. Hashizume, K, Yoshikawa, H, Morita, M and Suzuki, K (1985). Properties of attenuated mutant of vaccinia virus, LC16m8, derived from Lister strain. In: Quinnan GV, ed. *Vaccinia Virus as Vectors for Vaccine Antigens*. Elsevier Science: Amsterdam, pp 421–428.
6. Kenner, J, Cameron, F, Empig, C, Jobes, DV and Gurwith, M (2006). LC16m8: an attenuated smallpox vaccine. *Vaccine* **24**: 7009–7022.
7. Saito, T, Fujii, T, Kanatani, Y, Saijo, M, Morikawa, S, Yokote, H *et al.* (2009). Clinical and immunological response to attenuated tissue-cultured smallpox vaccine LC16m8. *JAMA* **301**: 1025–1033.
8. Yamaguchi, M, Kimura, M and Hirayama, M (1975). Report of the National Smallpox Vaccination Research Committee: Study of side effects, complications and their treatments. *Clin Virol* **3**: 269–278.
9. Morikawa, S, Sakiyama, T, Hasegawa, H, Saijo, M, Maeda, A, Kurane, I *et al.* (2005). An attenuated LC16m8 smallpox vaccine: analysis of full-genome sequence and induction of immune protection. *J Virol* **79**: 11873–11891.
10. Takahashi-Nishimaki, F, Funahashi, S, Miki, K, Hashizume, S and Sugimoto, M (1991). Regulation of plaque size and host range by a vaccinia virus gene related to complement system proteins. *Virology* **181**: 158–164.
11. Engelstad, M and Smith, GL (1993). The vaccinia virus 42-kDa envelope protein is required for the envelopment and egress of extracellular virus and for virus virulence. *Virology* **194**: 627–637.
12. Hollinshead, M, Rodger, G, Van Eijl, H, Law, M, Hollinshead, R, Vaux, DJ *et al.* (2001). Vaccinia virus utilizes microtubules for movement to the cell surface. *J Cell Biol* **154**: 389–402.
13. Katz, E, Ward, BM, Weisberg, AS and Moss, B (2003). Mutations in the vaccinia virus A33R and B5R envelope proteins that enhance release of extracellular virions and eliminate formation of actin-containing microvilli without preventing tyrosine phosphorylation of the A36R protein. *J Virol* **77**: 12266–12275.
14. Newsome, TP, Scaplehorn, N and Way, M (2004). SRC mediates a switch from microtubule- to actin-based motility of vaccinia virus. *Science* **306**: 124–129.
15. Rietdorf, J, Ploubidou, A, Reckmann, I, Holmström, A, Frischknecht, F, Zettl, M *et al.* (2001). Kinesin-dependent movement on microtubules precedes actin-based motility of vaccinia virus. *Nat Cell Biol* **3**: 992–1000.
16. Schmelz, M, Sodeik, B, Ericsson, M, Wolffe, EJ, Shida, H, Hiller, G *et al.* (1994). Assembly of vaccinia virus: the second wrapping cisterna is derived from the trans Golgi network. *J Virol* **68**: 130–147.
17. Smith, GL, Vanderplasschen, A and Law, M (2002). The formation and function of extracellular enveloped vaccinia virus. *J Gen Virol* **83**(Pt 12): 2915–2931.
18. Ward, BM and Moss, B (2001). Visualization of intracellular movement of vaccinia virus virions containing a green fluorescent protein-B5R membrane protein chimera. *J Virol* **75**: 4802–4813.
19. Wolffe, EJ, Isaacs, SN and Moss, B (1993). Deletion of the vaccinia virus B5R gene encoding a 42-kilodalton membrane glycoprotein inhibits extracellular virus envelope formation and dissemination. *J Virol* **67**: 4732–4741.
20. Kidokoro, M, Tashiro, M and Shida, H (2005). Genetically stable and fully effective smallpox vaccine strain constructed from highly attenuated vaccinia LC16m8. *Proc Natl Acad Sci USA* **102**: 4152–4157.
21. Kuruppu, D and Tanabe, KK (2005). Viral oncolysis by herpes simplex virus and other viruses. *Cancer Biol Ther* **4**: 524–531.
22. Mathis, JM, Stoff-Khalili, MA and Curiel, DT (2005). Oncolytic adenoviruses - selective retargeting to tumor cells. *Oncogene* **24**: 7775–7791.
23. Cawood, R, Chen, HH, Carroll, F, Bazan-Peregrino, M, van Rooijen, N and Seymour, LW (2009). Use of tissue-specific microRNA to control pathology of wild-type adenovirus without attenuation of its ability to kill cancer cells. *PLoS Pathog* **5**: e1000440.
24. Lee, CY, Rennie, PS and Jia, WW (2009). MicroRNA regulation of oncolytic herpes simplex virus-1 for selective killing of prostate cancer cells. *Clin Cancer Res* **15**: 5126–5135.
25. Edge, RE, Falls, TJ, Brown, CW, Lichty, BD, Atkins, H and Bell, JC (2008). A let-7 MicroRNA-sensitive vesicular stomatitis virus demonstrates tumor-specific replication. *Mol Ther* **16**: 1437–1443.
26. Kelly, EJ, Hadac, EM, Greiner, S and Russell, SJ (2008). Engineering microRNA responsiveness to decrease virus pathogenicity. *Nat Med* **14**: 1278–1283.
27. Lagos-Quintana, M, Rauhut, R, Lendeckel, W and Tuschl, T (2001). Identification of novel genes coding for small expressed RNAs. *Science* **294**: 853–858.
28. Zeng, Y, Yi, R and Cullen, BR (2003). MicroRNAs and small interfering RNAs can inhibit mRNA expression by similar mechanisms. *Proc Natl Acad Sci USA* **100**: 9779–9784.
29. Lagos-Quintana, M, Rauhut, R, Yalcin, A, Meyer, J, Lendeckel, W and Tuschl, T (2002). Identification of tissue-specific microRNAs from mouse. *Curr Biol* **12**: 735–739.
30. Chen, CZ (2005). MicroRNAs as oncogenes and tumor suppressors. *N Engl J Med* **353**: 1768–1771.
31. Sempere, LF, Christensen, M, Silahtaroglu, A, Bak, M, Heath, CV, Schwartz, G *et al.* (2007). Altered MicroRNA expression confined to specific epithelial cell subpopulations in breast cancer. *Cancer Res* **67**: 11612–11620.
32. Gramantieri, L, Ferracin, M, Fornari, F, Veronese, A, Sabbioni, S, Liu, CG *et al.* (2007). Cyclin G1 is a target of miR-122a, a microRNA frequently down-regulated in human hepatocellular carcinoma. *Cancer Res* **67**: 6092–6099.

33. Takamizawa, J, Konishi, H, Yanagisawa, K, Tomida, S, Osada, H, Endoh, H *et al.* (2004). Reduced expression of the let-7 microRNAs in human lung cancers in association with shortened postoperative survival. *Cancer Res* **64**: 3753–3756.
34. Johnson, SM, Grosshans, H, Shingara, J, Byrom, M, Jarvis, R, Cheng, A *et al.* (2005). RAS is regulated by the let-7 microRNA family. *Cell* **120**: 635–647.
35. Müller, DW and Bosserhoff, AK (2008). Integrin beta 3 expression is regulated by let-7a miRNA in malignant melanoma. *Oncogene* **27**: 6698–6706.
36. Torrisani, J, Bournet, B, du Rieu, MC, Bouisson, M, Souque, A, Escourrou, J *et al.* (2009). let-7 MicroRNA transfer in pancreatic cancer-derived cells inhibits *in vitro* cell proliferation but fails to alter tumor progression. *Hum Gene Ther* **20**: 831–844.
37. Barnes, D, Kunitomi, M, Vignuzzi, M, Saksela, K and Andino, R (2008). Harnessing endogenous miRNAs to control virus tissue tropism as a strategy for developing attenuated virus vaccines. *Cell Host Microbe* **4**: 239–248.
38. Pasquinelli, AE, Reinhart, BJ, Slack, F, Martindale, MQ, Kuroda, MI, Maller, B *et al.* (2000). Conservation of the sequence and temporal expression of let-7 heterochronic regulatory RNA. *Nature* **408**: 86–89.
39. Bell, E, Shamim, M, Whitbeck, JC, Sfyroera, G, Lambris, JD and Isaacs, SN (2004). Antibodies against the extracellular enveloped virus B5R protein are mainly responsible for the EEV neutralizing capacity of vaccinia immune globulin. *Virology* **325**: 425–431.
40. Pütz, MM, Midgley, CM, Law, M and Smith, GL (2006). Quantification of antibody responses against multiple antigens of the two infectious forms of Vaccinia virus provides a benchmark for smallpox vaccination. *Nat Med* **12**: 1310–1315.
41. Vanderplasschen, A, Mathew, E, Hollinshead, M, Sim, RB and Smith, GL (1998). Extracellular enveloped vaccinia virus is resistant to complement because of incorporation of host complement control proteins into its envelope. *Proc Natl Acad Sci USA* **95**: 7544–7549.
42. Kirn, DH, Wang, Y, Liang, W, Contag, CH and Thorne, SH (2008). Enhancing poxvirus oncolytic effects through increased spread and immune evasion. *Cancer Res* **68**: 2071–2075.
43. Brown, BD, Gentner, B, Cantore, A, Colleoni, S, Amendola, M, Zingale, A *et al.* (2007). Endogenous microRNA can be broadly exploited to regulate transgene expression according to tissue, lineage and differentiation state. *Nat Biotechnol* **25**: 1457–1467.
44. Kelly, EJ, Hadac, EM, Cullen, BR and Russell, SJ (2010). MicroRNA antagonism of the picornaviral life cycle: alternative mechanisms of interference. *PLoS Pathog* **6**: e1000820.
45. Czauderna, F, Santel, A, Hinz, M, Fechtner, M, Durieux, B, Fisch, G *et al.* (2003). Inducible shRNA expression for application in a prostate cancer mouse model. *Nucleic Acids Res* **31**: e127.
46. Haraguchi, T, Ozaki, Y and Iba, H (2009). Vectors expressing efficient RNA decoys achieve the long-term suppression of specific microRNA activity in mammalian cells. *Nucleic Acids Res* **37**: e43.

Nuclear and cytoplasmic effects of human CRM1 on HIV-1 production in rat cells

Mika Nagai-Fukataki[1], Takashi Ohashi[1], Iwao Hashimoto[2], Tominori Kimura[3], Yoshiyuki Hakata[1a] and Hisatoshi Shida[1]*

[1]*Institute for Genetic Medicine, Hokkaido University, Kita-ku, Sapporo 060-0815, Japan*
[2]*Department of Microbiology, Kansai Medical University, Moriguchi, Osaka 570-8506, Japan*
[3]*Laboratory of Microbiology and Cell Biology, College of Pharmaceutical Sciences, Ritsumeikan University, Kusatsu, Shiga 525-8577, Japan*

The human immunodeficiency virus type 1 (HIV-1) regulatory protein, Rev, mediates the nuclear export of unspliced *gag* and singly spliced *env* mRNAs by bridging viral RNA and the export receptor, CRM1. Recently, rat CRM1 was found to be less efficient than human CRM1 in supporting Rev function in rats. In this study, to understand the role of CRM1 in HIV propagation, the mechanism underlying the function of human and rat CRM1 in HIV-1 replication was investigated in rat cells. The production of viral particles, represented by the p24 Gag protein, was greatly enhanced by hCRM1 expression in rat cells; however, this effect was not simply because of the enhanced export of *gag* mRNA. The translation initiation rate of *gag* mRNA was not increased, nor was the Gag protein stabilized in the presence of hCRM1. However, the processing of the p55 Gag precursor and the release of viral particles were facilitated. These results indicated that hCRM1 exports *gag* mRNA to the cytoplasm, not only more efficiently than rCRM1 but also correctly, leading to efficient processing of Gag proteins and particle formation.

Introduction

Appropriate animal models for viral infection allow the analysis of viral pathogenesis and oncogenesis, which in turn assist the development of therapeutic and preventative measures. Current animal models of HIV-1 (human immunodeficiency virus-1) disease have used nonhuman primates (Giuffre *et al.* 2003; Hazuda *et al.* 2004; Hu 2005; Veazey *et al.* 2005) and severe combined immunodeficiency mice with transplanted fetal human tissues (Shultz *et al.* 2007; Watanabe *et al.* 2007). These models have made significant contributions to our understanding of lentiviral pathogenesis and have assisted in the development of therapeutic strategies. However, these models have significant shortcomings, such as the limited availability and high cost of nonhuman primates, the absence of or delay in disease progression, permissivity only for related retroviruses and insufficient viral propagation. For these reasons, new animal models are needed. If viral infection is possible, it would be convenient to use small animal models, in particular mice and rats, as their inbred strains are well characterized and can be genetically manipulated.

Studies on rodent cell-specific defects in the HIV-1 life cycle have facilitated the identification and characterization of the host cell gene products that are essential for viral replication, and these may provide a molecular basis for generating a fully permissive small-animal model. It has been suggested that the major block to HIV-1 replication is at the level of entry and that this hurdle could be overcome by introducing human CD4 and CCR5, which serve as receptors for HIV-1 (Keppler *et al.* 2001, 2002). Transgenic (Tg) rats, expressing human CD4 and CCR5, have been reported to support some replication of HIV-1, albeit very poorly (Keppler *et al.* 2002; Goffinet *et al.* 2007). In contrast, Tg mice

Communicated by: Haruhiko Siomi
**Correspondence*: hshida@igm.hokudai.ac.jp
[a]*Present address*: Department of Immunology, Kinki University School of Medicine, 377-2 Ohno-Higashi, Osaka-sayama, Osaka 589-8511, Japan.

DOI: 10.1111/j.1365-2443.2010.01476.x

expressing human CD4/CCR5 do not allow the propagation of HIV-1 (Browning *et al.* 1997). These results support the rat as a promising small-animal model candidate.

Analyses have showed novel interactions between rodent and viral factors. A notable example is CRM1 (chromosome region maintenance 1; exportin 1), a member of the karyopherin family of nucleocytoplasmic-transport factors (Neville *et al.* 1997; Cullen 2003) that is involved in nuclear export. In the nucleus, CRM1 binds its cargo in the presence of a GTP-bound form of the Ran GTPase (RanGTP), and following nuclear export, hydrolysis of GTP to GDP causes a conformational shift that induces cytoplasmic cargo release, providing directionality for this export pathway (Fornerod *et al.* 1997; Neville *et al.* 1997; Nakielny & Dreyfuss 1999; Cullen 2003). Human CRM1 cooperates with HIV-1 Rev and the human T cell leukemia virus type 1 (HTLV-1) Rex proteins to transport 4 kb of partially spliced and 9 kb of unspliced mRNAs encoding viral structural proteins and genomes (Cullen 1998). Rev or Rex multimerizes on viral RNA to recruit several CRM1 molecules; furthermore, the recruitment of CRM1 enhances Rev or Rex interactions vice versa (Hakata *et al.* 2002). Rat CRM1, which exhibits 98% amino acid identity to its human counterpart, is able to bind efficiently to Rex, but cannot induce the multimerization of Rex proteins on its cognate RNA. This results in the breakdown of HTLV-1 RNA transport in rat cells (Hakata *et al.* 2001). Thus, rat CRM1 represents a major factor in the human–rat species barrier to HTLV-1 (Zhang *et al.* 2006; Takayanagi *et al.* 2007). Furthermore, detailed comparisons of human and rat CRM1 proteins identified the domains essential for the induction of Rex multimerization and the binding of RanBP3, another component involved in RNA export (Hakata *et al.* 2003). These analyses suggested that CRM1 functions not only in RNA export out of the nucleus but also in the formation of the transport complex that includes viral RNA and various cellular components (Hakata *et al.* 2003).

In contrast to the definitive results obtained for rat CRM1-Rex interactions, the existence of a profound block in Rev function in rodent cells remains controversial, although a reduced level of the 9-kb transcript has been generally reported (Bieniasz & Cullen 2000; Keppler *et al.* 2001). Some studies have found impaired Rev activity (Marques *et al.* 2003), whereas others have ascribed the reduced transcript level to oversplicing or to the reduced stability of unspliced transcripts in rodent cells compared to human cells (Malim *et al.* 1991), a problem that is corrected by the expression of the human p32 protein (Zheng *et al.* 2003). These contradictory results seem to stem partly from the use of different cells and reporters for evaluating Rev activity and partly from the limited investigation of cellular cofactors. However, recently, we found that Gag production was increased by hCRM1 in rat macrophages in contrast to its marginal effect in rat T cells (Okada *et al.* 2009).

In this study, we have compared the molecular mechanisms underlying the function of human and rat CRM1 proteins in HIV propagation in rat cells. We show that the expression of hCRM1 in rat cells not only enhances the export of HIV *gag* mRNA but also restores the processing of the precursor Gag protein and release of viral particles, leading to efficient virus production.

Results

Enhanced p24 production in hCRM1-transfected rat cells

Recently, we found that hCRM1 enhanced Gag production in rat macrophages (Okada *et al.* 2009); therefore, it was decided to examine the molecular mechanism involved in this process using convenient rat cell lines. ER1/neo1 cells are particularly useful because they, like rat macrophages, support the efficient expression of HIV-1 genes without the need for human cyclin T1 (unpublished results [Okada *et al.* 2009;]). The initial step involved transfecting the hCRM1-expressing plasmid into ER1/neo1 cells along with the reporter pCRRE (Kimura *et al.* 1996), which harbors the HIV-1 genome, including the intact *gag* and *rev* sequences (Fig. 1A). Next, the production of the Gag protein, p24, in the medium was measured by ELISA. In addition, cells were simultaneously cotransfected with pCDMβ-gal, which was used to normalize the transfection efficiency, and pH1-luc, which acted as a surrogate marker for total gene expression driven by the HIV-1 LTR. In comparison with untransfected rat cells, hCRM1-transfected cells produced increasing levels of p24 in the culture supernatant with increasing amounts of pSRαhCRM1. On the other hand, β-gal and luc activities remained at similar levels in both hCRM1-transfected and untransfected rat cells, indicating similar transfection efficiencies and HIV LTR-mediated transcription, irrespective of hCRM1 expression (Fig. 1B). These results showed the enhancement of p24 production after transfection with hCRM1.

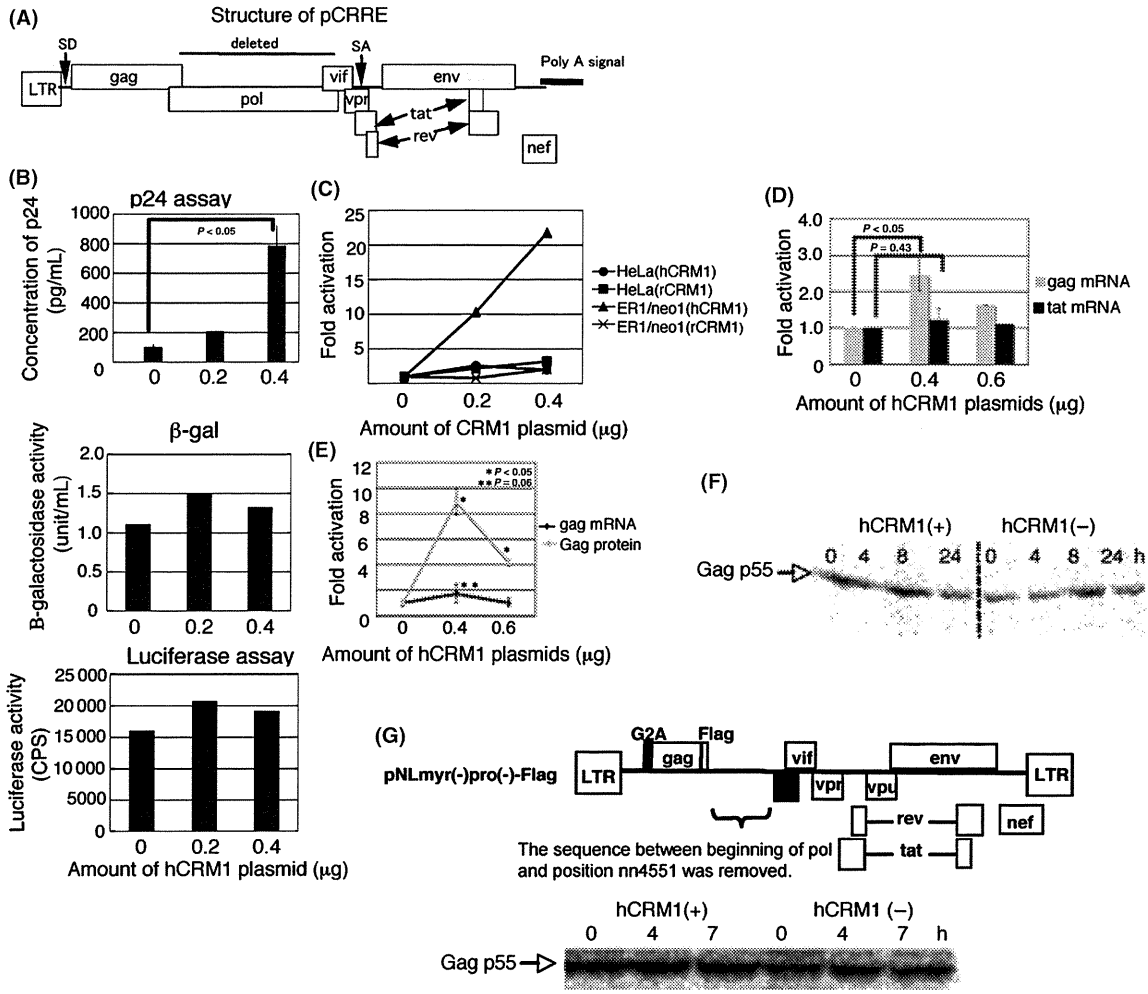

Figure 1 Effect of CRM1 on p24 production. (A) The structure of pCRRE. (B) ER1/neo1 cells (1×10^5) were transfected with 1.6 μg of pCRRE and pSRαhCRM1 as indicated, 0.1 μg of pCDMβ-gal, and 0.3 μg of pH1-luc using TransIT-LT1 (Mirus) reagent. The total abundance of transfected plasmids was adjusted with pSRα296. Two days after transfection, p24 was quantified from the cell culture medium using a RETRO-TEK HIV-1 p24 Antigen ELISA kit (ZeptoMetrix). Cytoplasmic β-gal activity was measured using standard colorimetric methods (β-gal assay) (Hakata *et al.* 2001), and luciferase activities were also quantified. (C) ER1/neo1 and HeLa cells were transfected with pCRRE, pCDMβ-gal and pH1-luc along with pSRαhCRM1 or pSRαrCRM1 as described earlier. The amount of p24 in the medium was quantified as in (B). The value of the control sample without CRM1 was set at 1. The β-galactosidase and luciferase activities were similar in all samples (data not shown). These data are representative of three independent experiments. (D) The amount of mRNA in cytoplasmic fraction in ER1/neo1 cells was indicated. ER1/neo1 cells were transfected with pCRRE, pSRαhCRM1, pCDMβ-gal and pH1-luc and then separated into nuclear and cytoplasmic fractions using an NP40 detergent-containing buffer, as described in Materials and Methods. Quantitative RT-PCR was used to determine the abundance of *gag*, *tat* and *β-gal* mRNAs in each fraction. The ratios of *gag* mRNA/*β-gal* mRNA and *tat* mRNA/*β-gal* mRNA were calculated. The value of the control sample without hCRM1 was set at 1. These values are the means of three independent sets of experiments, and the SD was calculated. (E) Gag protein (p24) in the medium and β-gal activity were quantified, and the Gag/β-gal ratio was plotted and compared to the ratio of cytoplasmic *gag* mRNA/*β-gal* mRNA. These data are representative of three independent experiments. (F) Stability of Gag protein in rat cells. At 48 h post-transfection, cells were pulse-labeled with [^{35}S]-methionine/cysteine and chased for 0, 4, 8 and 24 h. The medium and cells were solubilized with detergent-containing buffer and combined. Then, Gag proteins were immunoprecipitated using anti-Gag antibodies and protein-G Sepharose and analyzed by SDS–PAGE followed by autoradiography. (G) ER1/neo1 cells were transfected with pNLmyr(−)pro(−)Flag, pSRαhCRM1 and pCDMβ-gal. At 40 h post-transfection, cells were pulse-labeled with [^{35}S]-methionine/cysteine and chased for 0, 4 and 7 h. Gag proteins in the cell lysates were immunoprecipitated using anti-FLAG antibodies and protein-G Sepharose.

Next, we compared the effect of hCRM1 and rCRM1 in HeLa and ER1/neo1 cells by measuring p24 production. After transfection of either of the CRM1-expressing plasmids into HeLa cells, a small enhancement of p24 production was observed, although the differences between rat and human CRM1 were not significant (Fig. 1C). In addition, the same results were obtained in other human cell lines, including 293T and HOS cells (data not shown). In contrast, p24 production increased markedly in ER1/neo1 cells after transfection with the hCRM1-expressing plasmid, whereas expression of rCRM1 had no detectable effect (Fig. 1C). As expected, no significant changes in β-gal or luc activities were observed after transfection with human and rat CRM1-expressing plasmids (data not shown). In addition, hCRM1 enhanced expression of Gag in other rat cell lines (REF52, W31, FPM-SV and NR8383 cells [Okada *et al.* 2009]), whereas rCRM1 did not (data not shown). These results suggested that rCRM1 is a poor cofactor for Rev.

Effect of hCRM1 on the export of *gag* mRNA

The aforementioned results indicated that hCRM1 enhanced p24 production in rat cells; thus, the next step was to examine the mechanism underlying this phenomenon. It is conceivable that hCRM1 may export *gag* mRNA more efficiently than rCRM1. To investigate this possibility, hCRM1- or mock-transfected cells were separated into their nuclear and cytoplasmic fractions, and *gag* mRNA levels in the cytoplasmic fractions were compared using quantitative RT-PCR. To confirm augmented levels of Gag protein in these hCRM1-transfected cells, the medium was collected and subjected to a p24 ELISA. In the cytoplasm of hCRM1-transfected rat cells, the increase in *gag* mRNA levels was two to three times that of the mock-transfectants. A similar increase in *gag* mRNA was also observed in the nuclear fraction in the presence of hCRM1 (data not shown). On the other hand, hCRM1 expression had no effect on *tat* mRNA levels, because CRM1 is not involved in that particular export pathway (Fig. 1D). No signals were detected in the samples that had not been subjected to a reverse transcriptase (RT) reaction (data not shown). Efficient separation of the cytosolic and nuclear fractions was confirmed by amplification of *β-actin* pre-mRNA, which was detected exclusively in the nuclear fraction (data not shown). In contrast to the small increase in *gag* mRNA levels in the cytoplasm, at its peak, the production of p24 from hCRM1-transfected rat cells was nine times greater than in the mock-transfectants (Fig. 1E). p24 Gag production and the efficiency of gag mRNA export was decreased by transfection of 0.6 μg hCRM1 expression plasmids (Fig. 1D,E). Too much hCRM1 may affect nuclear export adversely because of imbalance with other factors. These results showed that hCRM1 modestly enhanced *gag* mRNA export in rat cells but greatly increased Gag protein production, suggesting that hCRM1 may function in the cytoplasm.

Stability of Gag protein

Next, we examined whether hCRM1 has an effect on Gag protein stability. A [^{35}S]-methionine/cysteine pulse-chase analysis of the Gag protein was carried out in rat cells transfected with pCRRE. An inhibitor against HIV-1 protease was added to prevent processing of the Gag precursor, which would hamper the assessment of Gag stability. As Gag proteins are released as viral particles into the medium, the total amount of Gag protein in both the cell and the medium should be quantified to assess its stability. Thus, the total cell culture including both cell lysates and medium was dissolved with the detergent solution and then immunoprecipitated with an anti-p24 monoclonal antibody (mAb), followed by SDS–PAGE and autoradiography. The Gag protein was highly stable, irrespective of the presence or absence of hCRM1 (Fig. 1F). The stability of the Gag protein was ascertained using another plasmid, pNL-myr(−)pro(−)Flag, which exclusively expresses intracellular, nonmyristoylated p55 Gag because of a G2A mutation at the 5′ region of the *gag* gene (Kawada *et al.* 2008) (Fig. 1G). These results excluded the involvement of hCRM1 in Gag protein stability.

The small increase in intensity of p55 Gag bands in the presence of hCRM1 (Fig. 1F,G) corresponded to the enhancement of gag mRNA in the cytoplasm (Fig. 1D,E), suggesting that the efficiency of *gag* mRNA translation was not elevated by hCRM1 expression. It is consistent with the results of polyribosome analysis that indicated a constant rate of translation initiation irrespective of hCRM1 expression (Data S1, Fig. S1 in supporting information).

Effect of hCRM1 on the export of *gag* mRNA and p24 production using pCMVΔR8.2

Next, the effect of hCRM1 was examined further using the plasmid, pCMVΔR8.2, which generates

higher levels of Gag protein in the medium of ER1/neo1 cells, compared to other reporters, such as pCRRE. The results showed that pCMVΔR8.2 synthesized Gag at 20- to 30-fold higher levels in the presence of hCRM1 than in its absence (Fig. 2A). As with the other reporters, a slight increase in cytoplasmic *gag* mRNA levels was observed in the presence of hCRM1 (Fig. 2B), whereas *tat* and *β-gal* mRNA levels were not affected (Fig. 2C,D). A similar increase in *gag* mRNA was also observed in the nuclear fraction in the presence of hCRM1 (data not shown). Efficient separation of the cytosolic and nuclear fractions was confirmed by the amplification of *β-actin* pre-mRNA, which was detected exclusively in the nuclear fraction (Fig. 2E), and β-galactosidase (as a cytoplasmic marker), of which approximately 95% was detected in the cytoplasmic fraction (Fig. 2F).

FISH analysis of *gag* mRNA

As part of our further investigation into the effect of hCRM1 on the export of *gag* mRNA in rat cells, the intracellular distribution of *gag* mRNA was analyzed using a fluorescence *in situ* hybridization assay (FISH). As this method does not require the physical separation of the cytoplasmic and the nuclear fractions, it was possible to rule out the leakage of mRNAs from the nuclear fraction during the process. ER1/neo1 cells were cotransfected with pCMVΔR8.2 and pSRαhCRM1, pSRαrCRM1 or the pSRα296 control vector. The intracellular distribution of *gag* mRNA was visualized using a DIG-labeled minus strand DNA probe [nucleotides (nts) 964 to 798 of HIV-1_{NL4-3} provirus], which is complementary to the *gag* coding region. The *gag* mRNA was distributed throughout the nucleus and cytoplasm of some cells, but was confined to the nucleus of other cells, irrespective of hCRM1 or rCRM1 expression. Both patterns of *gag* mRNA distribution were observed in HeLa and ER1/hCRM1-7 cells, which constitutively express hCRM1 (Fig. 3A). Control experiments demonstrated that the signals detected were specific for HIV-1 *gag* mRNAs; first, mock-transfected cells exhibited no signal after hybridization with the same probe and second, hybridization with the plus strand

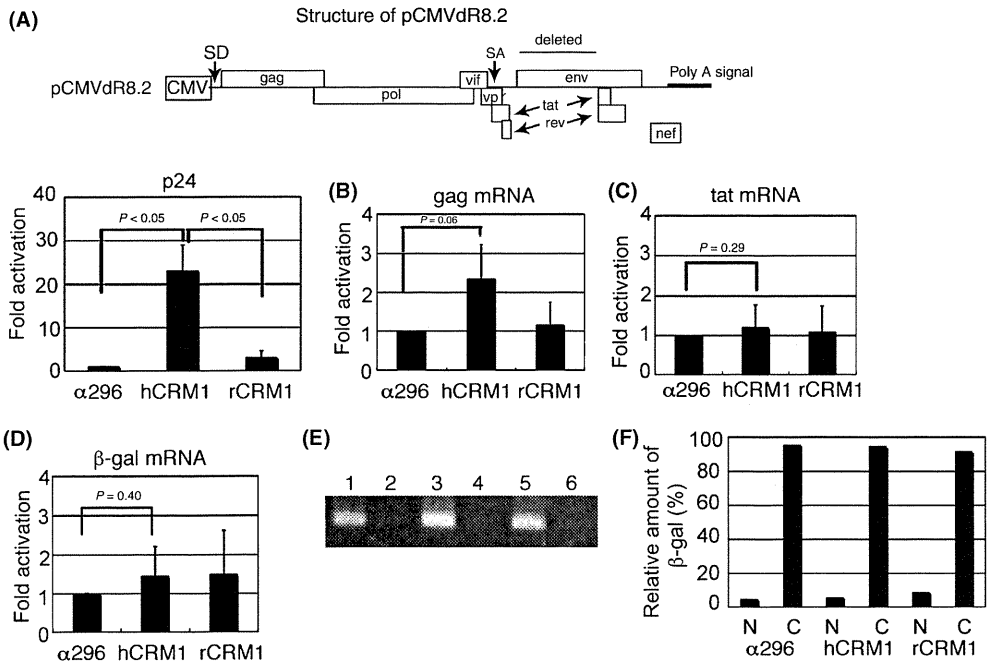

Figure 2 Effects of rat and human CRM1 on the production of Gag protein and *gag* mRNA derived from pCMVΔR8.2 in rat cells. (A–D) ER1/neo1 cells were transfected with pCMVΔR8.2 (1.6 μg) and pCDMβ-gal (0.1 μg) along with pSRαhCRM1 (0.4 μg) or pSRαrCRM1 (0.4 μg). The level of p24 in the medium and cytoplasmic β-gal activity, *gag* mRNA, *tat* mRNA and *β-gal* mRNA were quantified. The average and SD were calculated based on three independent sets of experiments. (E) PCR fragments of β-actin pre-mRNA in the nucleus (lanes 1, 3 and 5) and cytoplasm (lanes 2, 4 and 6) of cells without (lanes 1 and 2) or with (lanes 3 and 4) hCRM1 and (lane 5 and 6) rCRM1. (F) β-gal activity in the nuclear and cytoplasmic fractions was quantified, and the ratios of the β-gal activities in each fraction were calculated.

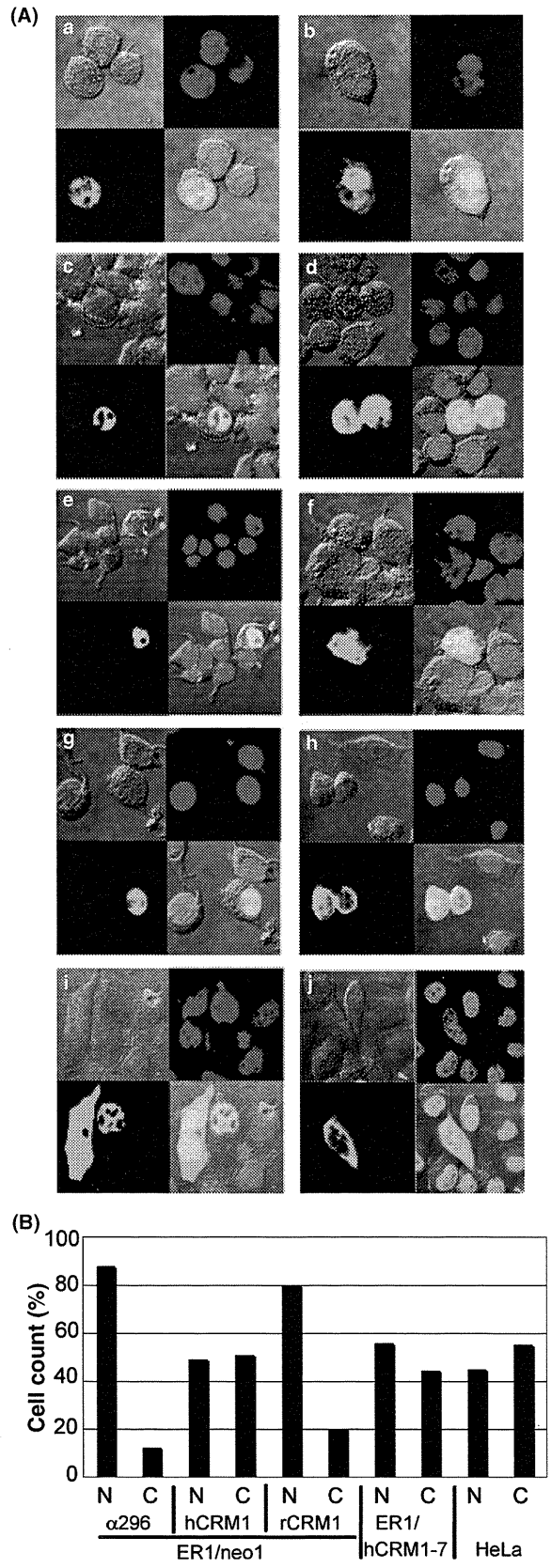

Figure 3 Fluorescence *in situ* hybridization (FISH) profiles of *gag* mRNA distribution in cells. (A) ER1/neo1 cells (panels a–f) were transfected with pCMVΔR8.2, along with pSRα296 (panels a and b), pSRαhCRM1 (panels c and d) or pSRαrCRM1 (panels e and f). ER1/hCRM1-7 (panels g and h) and HeLa cells (panels i and j) were transfected with pCMVΔR8.2. Cells were subjected to *in situ* hybridization. In all panels, the upper left image is phase contrast and the upper right shows DAPI-stained cells. The lower left image shows the FISH profile and the lower right is a merged image. (B) The number of cells (designated N) in which *gag* mRNA is localized exclusively to the nucleus and those (designated C) which contain *gag* mRNA distributed throughout the cytoplasm and nucleus. More than 150 cells were counted and their ratios are presented. These data represent the total number of cells counted in three independent experiments.

DNA probe (nts 798–964 of the HIV-1_{NL4-3} provirus) failed to show any signals in the transfected cells (data not shown). Fig. 3B shows the percentage of cells positive for the nuclear or cytoplasmic accumulation of *gag* mRNA. An approximately threefold increase in the cytoplasmic distribution of *gag* mRNA was observed in cells with constitutive or transient expression of hCRM1. These results were consistent with the quantification of cytoplasmic *gag* mRNA using RT-PCR (see Fig. 2B).

Effect of hCRM1 on the processing of Gag protein

We examined the processing of the Gag precursor and the release of viral particles using Western blot analysis. ER1/neo1 cells were transfected with pCMVΔR8.2, pCDMβ-gal and pSRαhCRM1-HA or pSRαrCRM1-HA as described earlier, and cell lysates and virus-like particle (VLP) fractions were prepared from the culture medium (Fig. 4A). The hCRM1 construct enhanced expression of the p55 Gag precursor approximately threefold, whereas it had a remarkable effect on the efficient processing of Gag (increasing it by approximately 10-fold) and on the formation of viral particles. The amount of VLP was evaluated by the p24 ELISA assay because the p24 bands of the VLP fractions, prepared from pSRα296 and pSRαrCRM1-transfected cells, were too faint in the Western blot profile to be quantified. The ELISA showed a 70-fold increase in VLP in response to the expression of hCRM1, whereas rCRM1 had no effect (data not shown). Less hCRM1 protein was expressed than rCRM1 protein (Fig. 4A), and it is possible that the hCRM1-HA protein may be unstable in ER1/neo1 cells, as shown

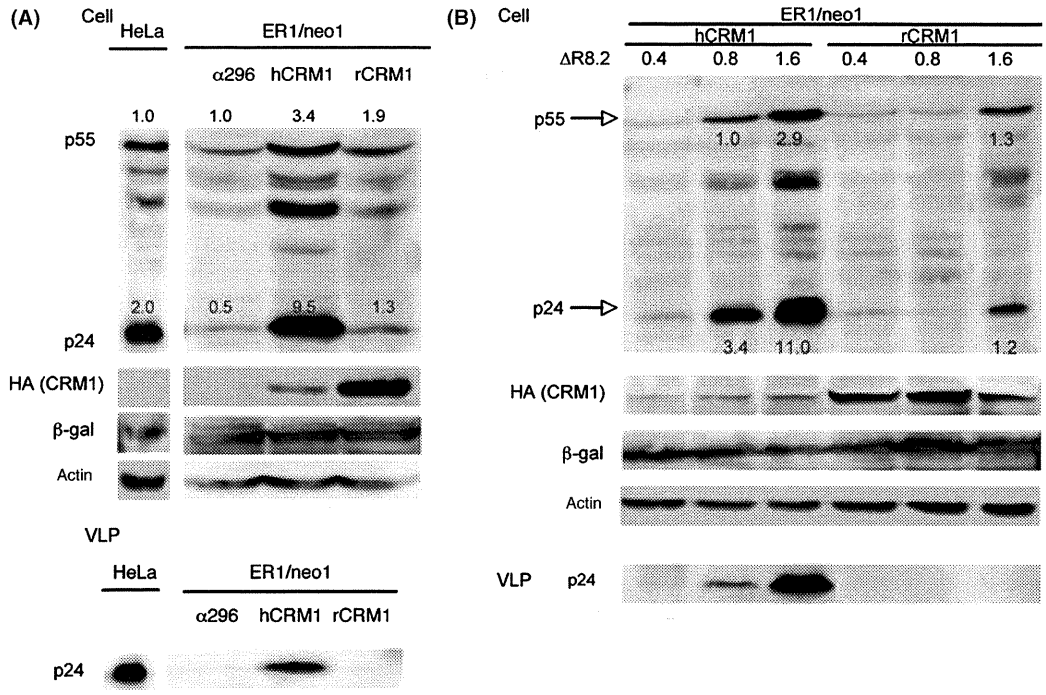

Figure 4 Western blotting of Gag proteins expressed in ER1/neo1 cells. (A) ER1/neo1 and HeLa cells were transfected with pCMVΔR8.2 and pCDMβ-gal along with the empty vector, pSRα296, and pSRαhCRM1-HA or pSRαrCRM1-HA as described earlier. Fractions corresponding to approximately 1.5×10^4 and 5×10^5 ER1/neo1 cells were subjected to Western blotting to analyze Gag protein profiles in the cell and VLP fractions, respectively. Fractions corresponding to approximately 5×10^3 and 5×10^4 HeLa cells were subjected to SDS–PAGE for analysis of the cell and VLP fractions, respectively. The intensities of the Gag proteins were quantified by LAS-1000. The amount of p55 Gag in pSRα296-transfected ER1/neo1 cells was set at 1.0, and the relative amounts of Gag protein were calculated. The ratio of p24/p55 expressed in HeLa was also presented. (B) ER1/neo1 cells were transfected with pCMVΔR8.2 (0.4–1.6 μg) and pCDMβ-gal (0.1 μg) along with pSRαhCRM1-HA (0.4 μg) or pSRαrCRM1 (0.4 μg). Fractions corresponding to approximately 2×10^4 and 5×10^5 cells were subjected to Western blotting to analyze Gag protein profiles in the cell and VLP fractions, respectively. The intensity of the p55 Gag band in the lane representing ER1/neo1 cells, transfected with 0.8 μg of pCMVΔR8.2 and pSRαhCRM1, was quantified and set at 1.0.

previously (Okada *et al.* 2009). The slight increase in p55 Gag protein in the presence of hCRM1 is consistent with the slight increase in *gag* mRNA observed in the cytoplasm (see Figs 1D,E and 2B). In addition, the remarkable increase in VLP is consistent with the increase in p24 detected by ELISA in the culture supernatant, as described earlier (Figs 1B and 2A). In human HeLa cells, which support high levels of HIV-1 production, both efficient processing and particle release were observed (Fig. 4A).

Next, to investigate whether the amount of Gag protein in the cells affected the processing of Gag and the release of viral particles, cells were transfected with various amounts of pCMVΔR8.2, together with pSRαhCRM1-HA or pSRαrCRM1-HA. The proportions of the p55 and p24 Gag proteins were similar, irrespective of the amount of p55 in the hCRM1-transfected cells (Fig. 4B). In contrast, the ratio of p24/p55 in the rCRM1-transfected cells was less than in the hCRM1-expressing cells, even when the rCRM1-transfected cells contained more p55. Moreover, the bands of p24 were clearly detected in the VLP fractions that were prepared from hCRM1-transfected cells, but not in the fractions from rCRM1-transfected cells (Fig. 4B). The relative amounts of p24, as quantified by ELISA, were 4.6, 59 and 1 in the VLP fractions of 0.8 μg pCMVΔR8.2/pSRαhCRM1-, 1.6 μg pCMVΔR8.2/pSRαhCRM1- and 0.8 μg pCMVΔR8.2/pSRαrCRM1-transfected cells, respectively (data not shown), consistent with the Western blotting profiles (Fig. 4B). These results suggested that the efficiency of Gag protein processing was enhanced by hCRM1-mediated *gag* gene expression but not by the amount of intracellular Gag protein.

Effect of hCRM1 on membrane trafficking and the release of p55 Gag

To examine the effect of hCRM1 on the destination of the Gag protein, in the absence of Gag processing, the p55 Gag protein was expressed using pNLmyr(−)pro(−)Flag and pNLmyr(+)pro(−)Flag because these vectors express only uncleaved p55, while the FLAG tag supports clear images in immunofluorescent assays. Moreover, the amount of p55 expressed by pNLmyr(−)pro(−)Flag may reflect the amount of *gag* mRNA in the cytoplasm more accurately because it is not released into the medium because of the lack of myristoylation.

When pNLmyr(−)pro(−)Flag was transfected into ER1/neo1 cells, hCRM1 expression augmented the amount of intracellular p55 by 3.3- or 2.5-fold more than the empty vector or rCRM1 expression, respectively (Fig. 5A). This moderate increase in p55 Gag protein in the presence of hCRM1 reflected the small enhancement of *gag* mRNA observed in the cytoplasm (see Figs 1D,E and 2B), consistent with the

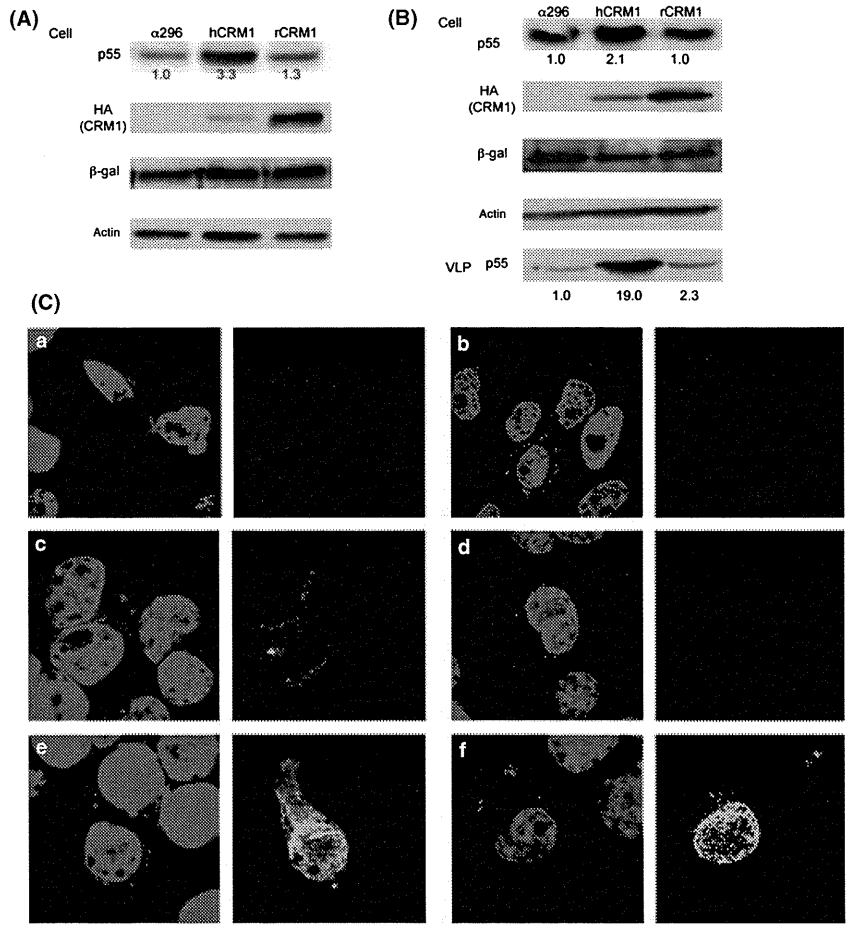

Figure 5 Effect of hCRM1 on membrane trafficking and release of virus particles using pNLmyr(−)pro(−)Flag and pNLmyr(+)pro(−)Flag. Approximately, 2×10^4 ER1/neo1 cells transfected with pNLmyr(−)pro(−)Flag along with pSRα296, pSRαhCRM1 or pSRαrCRM1 were subjected to Western blotting (A). The cells and VLP fractions corresponding to approximately 5×10^3 and 5×10^5 cells transfected with pNLmyr(±)pro(−)Flag along with pSRα296, pSRαhCRM1 or pSRαrCRM1 were subjected to Western blotting, respectively (B). The band intensity of p55 Gag expression in pSRα296-transfected cells was set at 1.0. (C) HeLa cells were transfected with pNLmyr(−)pro(−)Flag (panel a) or pNLmyr(+)pro(−)Flag (panel b). ER1/neo1 cells were transfected with pNLmyr(−)pro(−)Flag and pSRαhCRM1 (panel c), or pNLmyr(+)pro(−)Flag along with pSRα296 (panel d), pSRαhCRM1 (panel e), or pSRαrCRM1 (panel f). Cells were subjected to direct immunofluorescence assay. In all panels, the left image is a merged picture of DAPI (blue) and p55 Gag protein (red), and the right-hand panels show exogenous CRM1 (green).

results described in Fig. 1F,G and S1. When pNLmyr(+)pro(−)Flag was transfected into ER1/neo1 cells, hCRM1 expression enhanced the intracellular p55 level by twofold compared to the empty vector or rCRM1 expression. In contrast, hCRM1 expression augmented VLP production by 19- or 8-fold compared to the empty vector or rCRM1 expression, respectively (Fig. 5B). These results suggested that hCRM1 promotes the release of viral particles independent of the processing of p55.

Next, immunofluorescence was used to examine the localization of p55 Gag in the presence or absence of hCRM1. Unmyristoylated p55 was distributed diffusely throughout the cytoplasm of both HeLa and hCRM1-expressing ER1/neo1 cells transfected with pNLmyr(−)Gag-Flag (Fig. 5C panels a and c). On the other hand, myristoylated Gag was characterized by its punctate state on the plasma membranes of HeLa and ER1/neo1 cells transfected with pNLmyr(+)Gag-Flag, irrespective of the expression of human or rat CRM1 (Fig. 5C panels b, d, e and f). The ratio (20–30%) of rat cells that showed the punctate Gag profile was not increased by the expression of hCRM1, whereas almost HeLa cells showed the punctate profiles. These results suggest that the membrane trafficking of p55 Gag occurred in the rat cells inefficiently compared to the human cells and it was not restored by hCRM1.

Region of hCRM1 responsible for the up-regulation of p24 production

To identify the region of hCRM1 responsible for the production of p24, we compared the ability of the two chimeric CRM1s to produce p24: hrCRM1 consisted

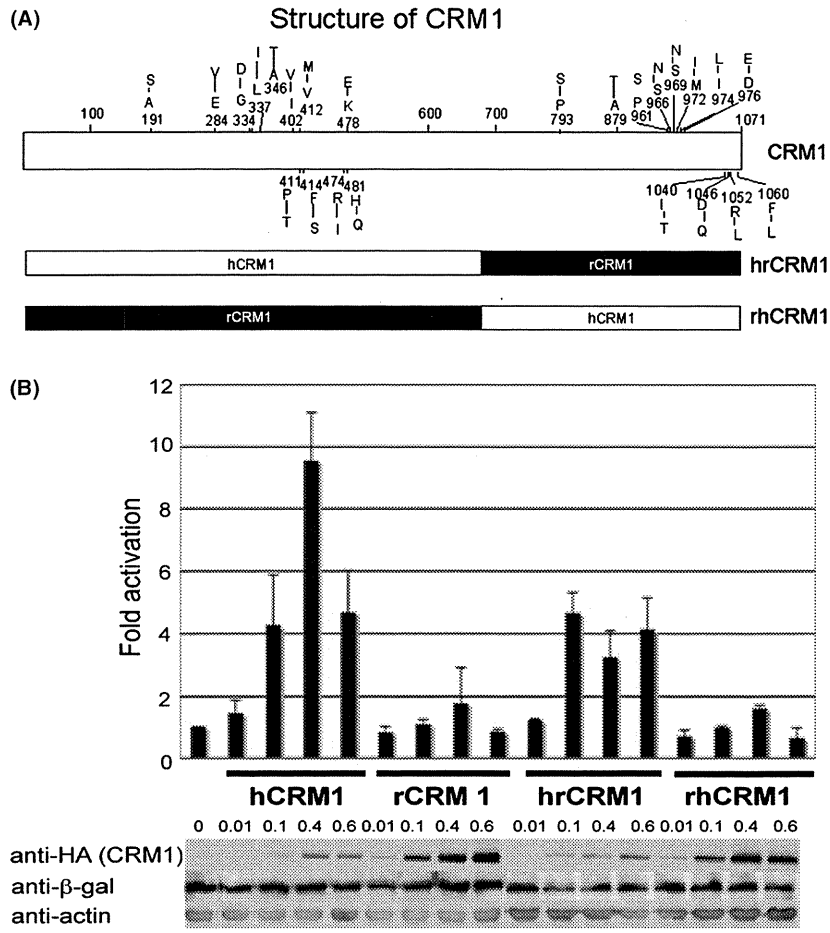

Figure 6 Analysis of the region of hCRM1 responsible for the up-regulation of p24 production in ER1/neo1 cells. (A) Structure of CRM1. (B) ER1/neo1 cells were transfected with pCMVΔR8.2, pCDMβ-gal and various CRM1-expressing plasmids. HIV-1 p24 in the medium was quantified by ELISA. The protein expression of CRM1, β-gal and actin was analyzed by Western blotting.